March 1968 USCEE Report 263

# UNIVERSITY OF SOUTHERN CALIFORNIA

FINAL REPORT

## MILLIMETER-WAVE RADIOMETRY FOR RADIO ASTRONOMY

W. V. T. Rusch
S. D. Slobin
C. T. Stelzried

Contract No. JPL 951756

Prepared for

JET PROPULSION LABORATORY
PASADENA, CALIFORNIA

## ELECTRONIC SCIENCES LABORATORY

March 1968

USCEE Report 263

# MILLIMETER-WAVE RADIOMETRY FOR RADIO ASTRONOMY

W. V. T. Rusch
S. D. Slobin
C. T. Stelzried

FINAL REPORT

Contract No. JPL 951756

This work was performed for the Jet Propulsion Laboratory, California Institute of Technology, sponsored by the National Aeronautics and Space Administration under Contract NAS7-100.

Prepared for

JET PROPULSION LABORATORY
PASADENA, CALIFORNIA

TABLE OF CONTENTS

## I. HISTORY OF THE PROGRAM

In September, 1963, the mm-wave instrumentation program was initiated as a joint effort between the Jet Propulsion Laboratory and the Electrical Engineering Department of the University of Southern California. The JPL participation was conducted through the New Circuit Elements Group of the Communications Elements Research Section, which provided equipment and personnel involved primarily with the electronic instrumentation.

The Electrical Engineering Department contributed the antenna, a converted 60-inch searchlight. Personnel were provided to design the antenna and feed system, the associated drive system, etc. USC personnel also directed the astronomical aspects of observation of the lunar eclipse of 30 December 1963. During this period, from September, 1963 to July, 1964 USC participation was sponsored by a grant from the Research Corporation, Contract AJ4-205 638 from JPL, and financial support for salaries and equipment from the Electrical Engineering Department Joint Services Grant, AF-AFOSR-496-64.

In August, 1964 a JPL study contract was issued to the USC Electrical Engineering Department (JPL Contract No. 951 004). This contract continued the previous work as a joint JPL-USC program. Under this contract observations were made of a lunar eclipse on 19 December 1964, a lunation study of the moon was made, instrumentation was developed, and various atmospheric effects were studied. A second JPL study contract was issued in October, 1965. Under this contract a second lunation experiment was carried out, the sun was observed, atmospheric effects continued to be studied, and various items of instrumentation were designed and studied.

A third JPL study contract was issued in November, 1965 for a period of one year, terminating in November, 1966. During the period of this contract Mr. Stephen Slobin, a graduate student at USC who has been associated with the joint JPL-USC Millimeter-wave program since its inception, carried out the analysis and development of a nodding subdish system (NSS). During this period Professor W. V. T. Rusch, principal investigator, was at the Bell Telephone Laboratories in New Jersey on leave of absence from the University. This third study contract was later extended an additional two months until 31 December, 1967 for the purposes of investigating theoretical and experimental radiometric techniques to measure atmospheric weather dependent parameters, and to study the effect of variable atmospheric conditions on lunation and eclipse sun and moon observations.

## II. INSTRUMENTATION

During the period of time covered by the various study contracts described in the previous section a 90-GHz (3.33 mm) radio telescope has been developed using a converted 60-inch searchlight as an antenna. Previous electronic systems used in the radio telescope were standard Dicke-type synchronous detection radiometers[1,2]. This radiometer scheme was used for measurements of lunar eclipses in 1963 and 1964, lunations in 1965 and 1966, and solar thermal emission studies.

The radiometer configuration used in the above studies required the use of a ferrite switching circulator or equivalent ferrite switching device in the RF path between the antenna feedhorn and the mixer. This device introduced considerable insertion loss (as high as 1 dB) in the main RF path, thereby degrading the sensitivity of the radiometer proportionately. Furthermore, it was anticipated that the operational frequency of the radiometer would be significantly increased at a later date, and the insertion loss of ferrite switching elements becomes prohibitive at shorter wavelengths.

Consequently a nodding subdish system (NSS) was developed which eliminated the ferrite device in the RF path and achieved the required switching by causing the antenna beam to alternate between the source being

[1] Rusch, W. V. T., S. Slobin, and C. T. Stelzried, "Millimeter-Wave Radiometry for Radio Astronomy," Final Report, USCEE Rept. 161, University of Southern California, Los Angeles, California, February 1966.

[2] Rusch, W. V. T., S. Slobin, and C. T. Stelzried, "Millimeter-Wave Radiometry for Radio Astronomy," Final Report, USCEE Rpt. 183, University of Southern California, Los Angeles, California, December 1966.

observed and a nearby position in the sky[2]. The beam-switching was accomplished by mechanically nutating the hyperboloidal subreflector in the Cassegrainian feed system between two symmetric but off-axis positions. A second advantage of this beam-switching configuration is the cancellation of long-term (relative to the switching rate) atmospheric noise scintillations when the scintillating area is included in both positions of the antenna beam. Preliminary descriptions of the NSS are given in the last final report.[2]

A. <u>Instrumentation Development.</u> An extensive series of mechanical tests was made to determine possible operating frequencies for the subdish mechanism, since mechanical problems would limit the maximum switching frequency of the system. Although operation of the subdish mechanism was made at rates as high as 8 cps, it was felt that this was mechanically punishing to the relatively delicate mechanism, which would have to operate for several million cycles without failure or repair. It was decided, after extensive electronic tests also, that 2.7 cps was a good compromise for optimum mechanical and electronic operation. High frequencies (greater than 5 cps) were poor from a mechanical standpoint, and low frequencies (less than 2 cps) were poor from an electronic standpoint. Consequently, the 90 GHz radiometer used in the present USC/JPL radio telescope was operated in a synchronous detection mode at a switching rate of 2.7 cps. The nodding subdish switched the beam back and forth and the net RF signal in phase with a 2.7 cps radiometer reference was synchronously detected.

A block diagram and photo of the RF portion of the radiometer are shown in figures II-1 and II-2. A block diagram and photo of the electronic system are shown in figures II-3 and II-4.

The subdish drive mechanism not only operates the subdish but also creates a square wave electrical signal for use as a radiometer reference input. The square wave signal is obtained by chopping a light beam with a rotating slotted wheel. This wheel may be rotated with respect to the drive shaft to adjust the phase relationship between subdish movement and radiometer reference. Testing indicated that the optical sensor in the drive mechanism did not give a sufficiently "square" wave to switch the AIL Radiometer properly. A Hewlett-Packard function generator was modified to receive the reference signal, square it, and present it to the AIL radiometer in a form suitable for proper operation. This square wave is also used as input to the ferrite switch drive, and switches the hot load signal at the synchronous frequency during calibration measurements.

To reduce RF signal loss and increase measurement sensitivity, the signal line from feedhorn to mixer was made as short and direct as possible. There are only three items in the RF signal line — the diagonal feedhorn, a TRG Model E-530 manual four-port waveguide switch, and a Baytron isolator, having a very low insertion loss (approximately 0.4 dB). The mixer is a Raytheon Model WR-10 balanced mixer. The diagonal feedhorn is well matched and introduces little loss in the system. The VSWR looking into the output port of the horn measured less than 1.05 over a frequency range from 89.60 GHz to 90.30 GHz.

The hot load calibration line consists of the heated waveguide termination contained within a thermally insulated aluminum box, a TRG Model E-162 switching circulator, the four-port waveguide switch, and the above mentioned Baytron Isolator. Both the hot load and the ambient load are fitted with Dymec Quartz Crystal Oscillators which enable the load temperatures to be measured to an accuracy of about 0.01$^{\circ}$K.

The local oscillator line consists of a Varian Model VC-113 Klystron, a TRG Model E-561 10-db directional coupler, an MCS Model Y-244 flap attenuator, a TRG Model E-550 frequency meter, and a TRG Model E-110 isolator.

The electronic system consists of an AIL Type 2392 Universal Radiometer, a TRG Model 171 ferrite switch driver, a Hewlett-Packard Model 203A function generator (used for squaring the subdish reference signal), a Dymec quartz thermometer, and other pieces of auxiliary equipment.

Short term (minutes) jitter of 3$^{\circ}$K peak-to-peak and long term (hours) jitter of 4$^{\circ}$K peak-to-peak were achieved with this radiometer system, operating at a switching rate of 2.7 cps, with a post-detection time constant of three seconds and a ten second digital voltmeter sampling period. This represents a threefold improvement over the previous radiometer system, which operated at 37 cps. The improvement does not arise solely from the use of a nodding subdish system but also from electronic and operational improvements in the radiometer itself.

B. Radiometer Noise and Gain Change Measurements. During radiometer testing to determine the optimum switching frequency for the nodding subdish mechanism, it became apparent that low frequency radiometer switching resulted in increased radiometer instability, noise jitter, and gain changes. It was decided to examine the radiometer performance at various switching frequencies to determine the amplitude and frequency dependence of these instabilities.

Noise in an idealized radiometer arises from contributions of two sources: 1) thermal noise jitter, and 2) gain changes. In a total power radiometer these contributions may be written as

$$\Delta T_{\substack{\text{thermal} \\ \text{total power}}} = \frac{K_1 T_s}{\sqrt{B\tau}} \tag{II-1}$$

$$\Delta T_{\substack{\text{gain change} \\ \text{total power}}} = K_2 \frac{\Delta G}{G} T_s \tag{II-2}$$

where $T_s$ = system temperature

$B$ = pre-detection bandwidth

$\tau$ = post-detection time constant

$G$ = receiver gain

In a Dicke radiometer, where the input signal arises from RF switching between source and reference, this may be written as:

$$\Delta T_{\substack{\text{thermal} \\ \text{Dicke}}} = \frac{K_3 T_s}{\sqrt{B\tau}} \qquad \text{(II-3)}$$

$$\Delta T_{\substack{\text{gain change} \\ \text{Dicke}}} = K_4 \frac{\Delta G}{G} (T_2 - T_1) \qquad \text{(II-4)}$$

The constants in Equations (II-1,2,3,4) are of the order of 1.

Since these noise temperatures are non-correlated,

$$\Delta T_{\text{Dicke}} = \sqrt{\left(K_3 \frac{T_s}{\sqrt{B\tau}}\right)^2 + \left(K_4 \frac{\Delta G}{G} [T_2 - T_1]\right)^2} \qquad \text{(II-5)}$$

The radiometer gain probability distributions may be represented (following Strum[3]) as in Figures II-5 and II-6. G is the gain of the radiometer, $G_o$ is the average again of the radiometer, P(G) is the probability distribution function of the radiometer gain, and f is the frequency of random gain fluctuations. Thus, Figure II-5 shows that the radiometer gain has some probability distribution centered about $G_o$; and Figure II-6 shows that most radiometer gain changes occur with low frequency. From these figures we can see that the faster the radiometer is switched between source and reference, the less effect gain instabilities have on increasing the noise of the radiometer, particularly if the term $(T_2 - T_1)$ is small. For high-speed switching, the term $\Delta T_{\text{gain change}}$ becomes negligible and the curve of

[3] Strum, Peter, "Considerations in High-Sensitivity Microwave Radiometry," Proceedings of the IRE, Vol. 46, No. 1, January 1958, pp. 43 ff.

$\Delta T_{Dicke}$ approaches the theoretical value for thermal noise jitter alone. Figure II-7 indicates schematically the relationships between switching frequency and noise jitter for an idealized Dicke radiometer system. Curves of $\Delta T$ vs. f may be drawn for various values of $(T_2 - T_1)$ as in Figure II-8.

A series of radiometer tests was made at various switching frequencies to determine the effects of thermal noise and gain changes. Radiometrically switching between a hot load and an ambient load yielded one of the curves in Figure II-8. Switching between two ambient loads yielded the dotted line, since $(T_2 - T_1)$ were equal to zero, and gain changes had no effect on the synchronously detected output. One must realize that this will only be true for an idealized Dicke radiometer system.

The experimental method used in these tests was to switch between the hot and ambient loads, and then between both ambient loads at different switching frequencies. $\Delta T$ is defined in this section as the actual probable error (in degrees Kelvin) in the measurement of the net detected power when switching between $T_2$ and $T_1$. For the radiometer performance tests, the physical temperature difference between the hot and ambient loads was approximately $60^{\circ}K$. However, since the output of the hot load must pass through the load waveguide, a four-port switch, and a ferrite switch, the net output difference was determined to be $35^{\circ}K$.

The results of the tests are shown in Figure II-9. Graphical representations of these results indicates that both the $\Delta T = 0$ and the $\Delta T \neq 0$ curves have a frequency-dependent character, whereas theoretically, only the $\Delta T \neq 0$ curve should have this characteristic. What the graphical results indicate, then, is that in the expression for $\Delta T$ containing the thermal jitter term and the gain stability term (Equation II-5), a third term $(\Delta T)_3$ must also be added. Thus, for a non-ideal Dicke radiometer,

$$\Delta T_{Dicke} = \sqrt{\left(K_3 \frac{T_s}{\sqrt{B\tau}}\right)^2 + \left(K_4 \frac{\Delta G}{G}[T_2 - T_1]\right)^2 + (\Delta T)_3^2}$$

The $(\Delta T)_3$ term increases with decreasing frequency and at frequencies below 5 cps begins to dominate the other two terms. Its domination may be clearly seen from the graph, since both $\Delta T$ curves have approximately the same shape and value for low frequencies. This also indicates that the contributions of the first two terms are quite small at low frequencies.

In many actual radiometric applications, switching rates in the Dicke system are high enough (greater than approximately 30 cps) to eliminate the effects of radiometer gain instabilities and other low frequency effects. Theoretically and practically, the problems associated with low-frequency Dicke switching are avoided. However, in low-frequency switching applications, it is necessary to consider all possible sources of radiometer instabilities — mixer diodes, local oscillator, IF amplifiers, switching transients, radiometer rear-end, etc. These areas may be considered subjects for intensive studies in the future.

In addition to the radiometer switching frequency tests, a second experiment was carried out to determine the noise power spectrum of the radiometer output. Figure II-10 indicates the apparatus utilized in this investigation. The RF signal was modulated by a ferrite switch, switching at 2.7 cps between a hot load and an ambient load. The amplified and detected IF signal was sampled directly without processing by the synchronous detector. The RF switching resulted in a 2.7-cps calibration pulse being inserted in the spectrum since the switching was indistinguishable from a 2.7 cps gain change. The amplitude of the calibration pulse was directly proportional to the net noise temperature difference ($T_2$-$T_1$) between the hot and ambient terminations. Figure II-11 indicates schematically the form of the spectral content of the noise. Figures II-12 and II-13 show the measured spectral content for the ranges 0-50 cps and 0-5 cps.

Reference to Figure II-1 will show that the magnitude of the 2.7 cps calibration pulse was determined by the equivalent output temperature of the hot load and the insertion loss of the waveguide run between the hot load and the output of the switching circulator. Insertion loss measurements gave a loss of 2.3 dB for the waveguide run including the switch port and circulator. The VSWR looking into the hot load was less than 1.03. Consequently, the equivalent output temperature of the hot load was 35$^{\circ}$K. This was the magnitude of the pulse relative to the curve in Figures II-13 and II-14. Thus, the minimum noise jitter attainable by the radiometer (at high switching frequencies) was about 1$^{\circ}$K.

C. Antenna Characteristics. A preliminary description of the NSS was given in the previous contract final report.[4] As indicated in that report, the subdish moves 2.06° to each side of its symmetric position (axis of hyperboloid colinear with axis of paraboloid). The total excursion from one extreme of tilt to the other is 4.12°. The total antenna beam shift between extremes is 55.5 minutes of arc. Hence, the deviation of the beam from its symmetric position is 27.75 minutes of arc. Static antenna patterns, measured with the subdish tilted to its off-axis position, are shown in Figures II-14 and II-15. Additional pattern measurements indicated that the 3-dB beamwidth in the East-West plane is 12.4 minutes of arc, and in the North-South plane is 9.7 minutes of arc.

The diagonal feedhorn was initially described in the last final report.[5] Measurements of the feedhorn pattern indicated a 13-dB taper at the edges of the illuminated hyperboloid (angular diameter is 19°). The 3-dB beamwidth of the horn pattern is 9.5°.

---

[4] Rusch, Slobin, Stelzried; op cit.

[5] Rusch, Slobin, Stelzried; ibid.

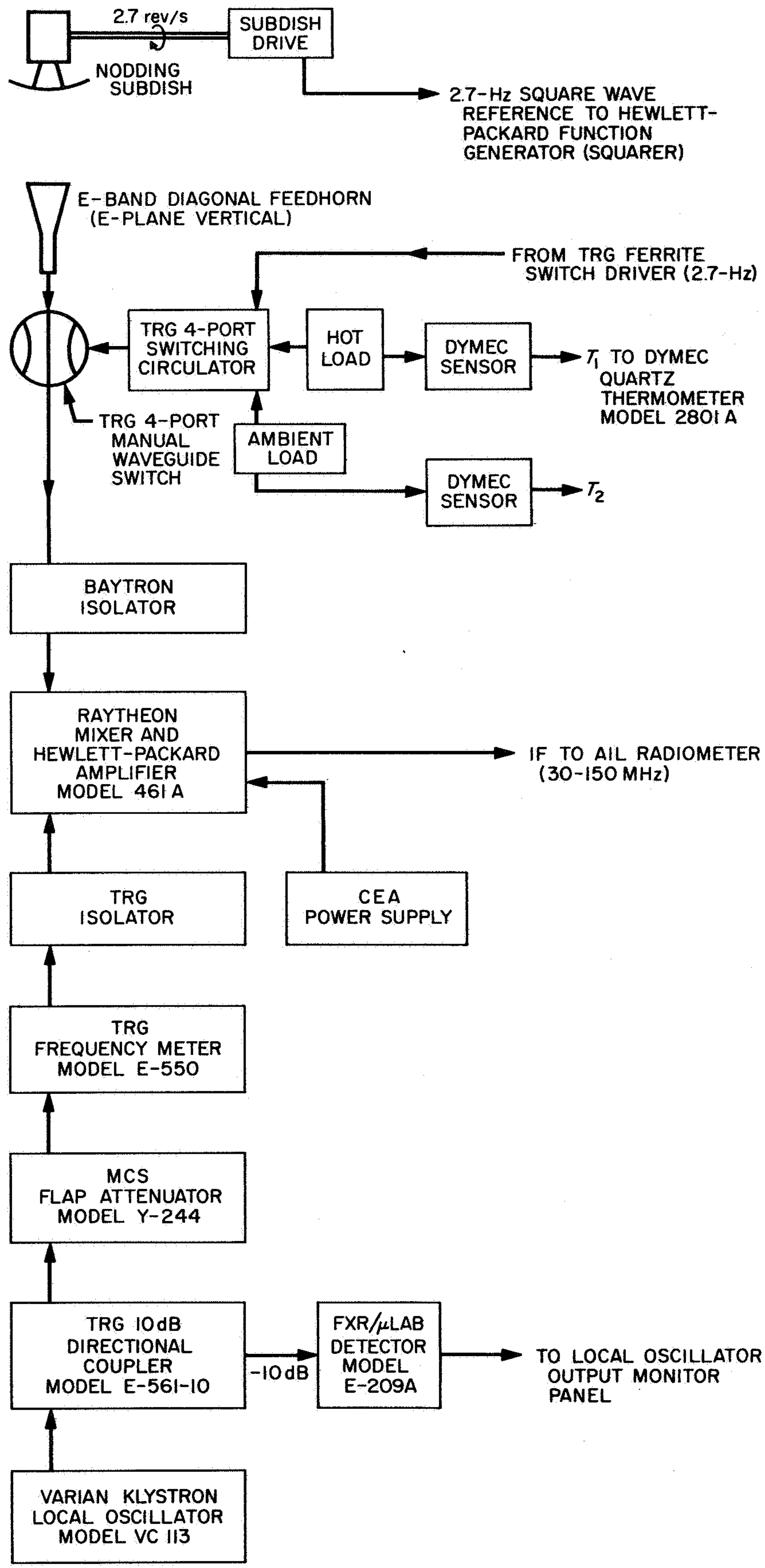


Figure II-1. Block diagram of RF portion of nodding subdish system.

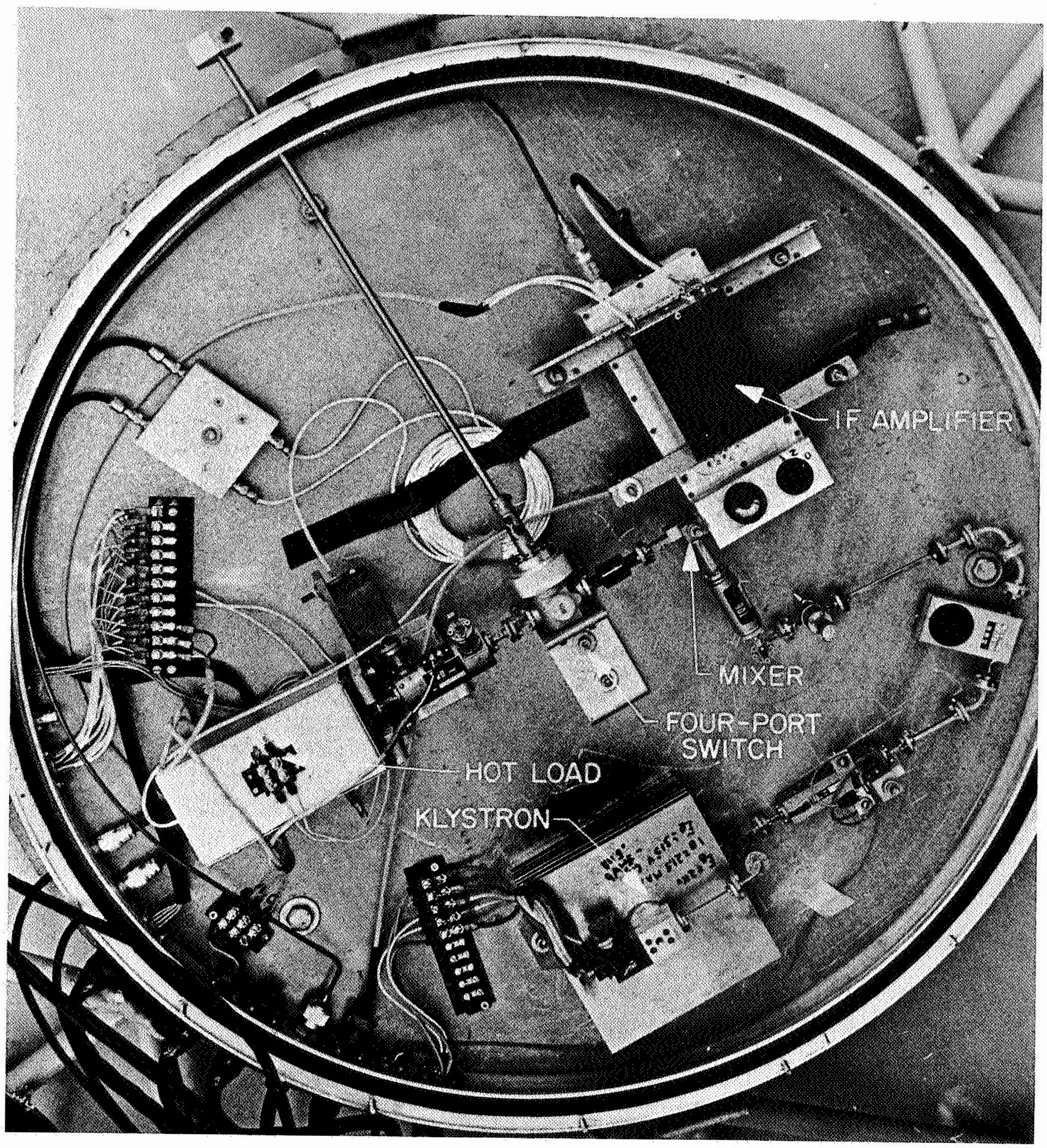


Figure II-2. Photo of RF portion of nodding subdish system.

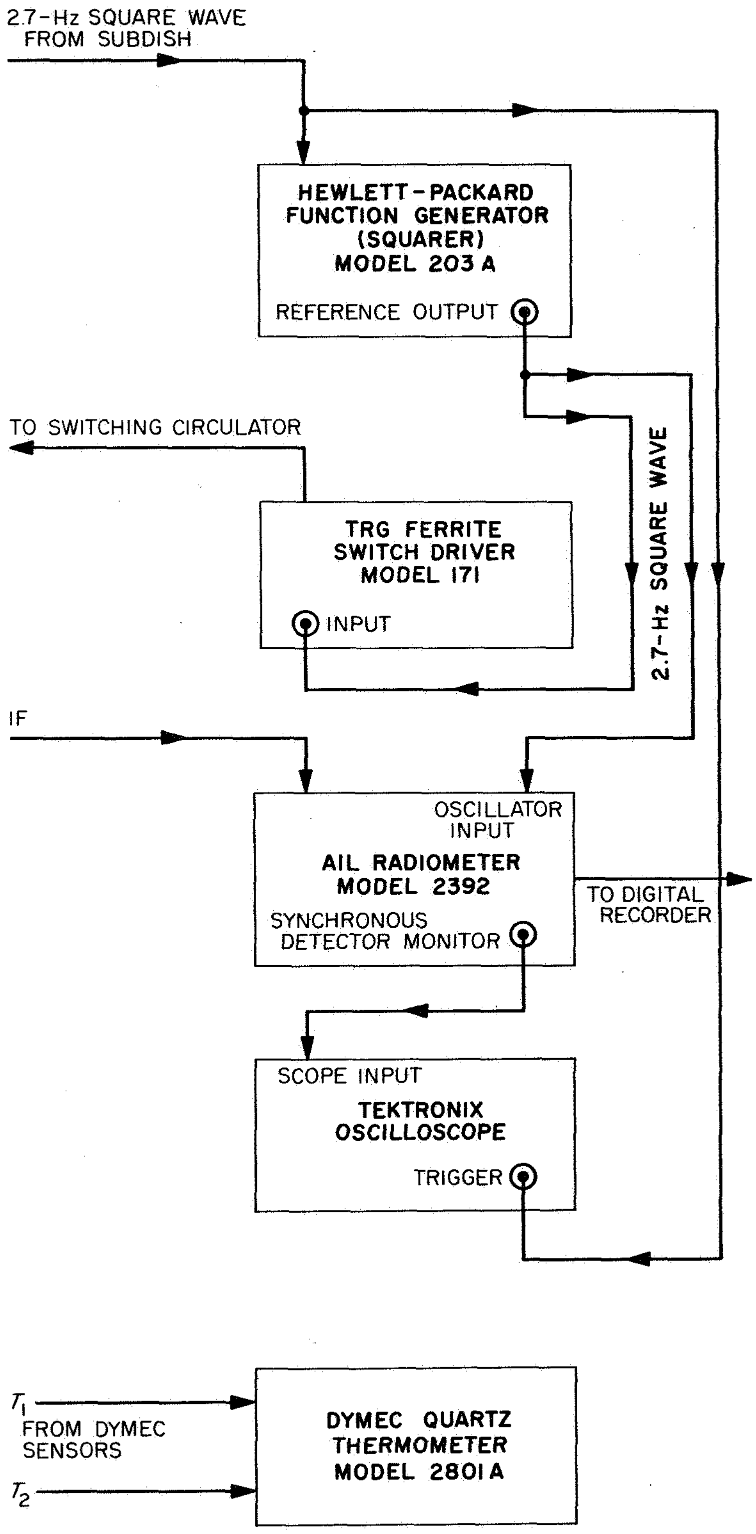


Figure II-3. Block diagram of electronic portion of nodding subdish system.

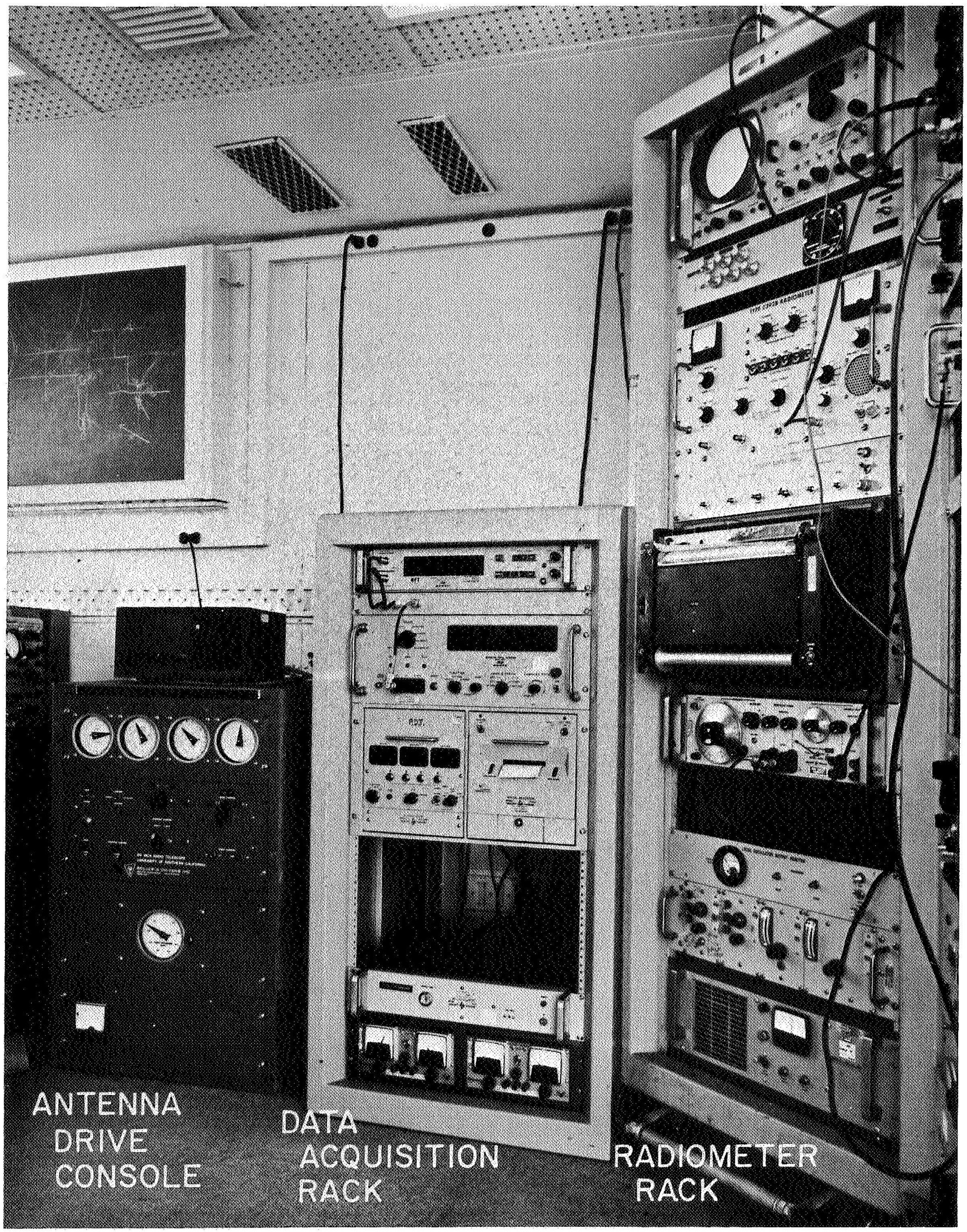


Figure II-4. Photo of electronic portion of nodding subdish system.

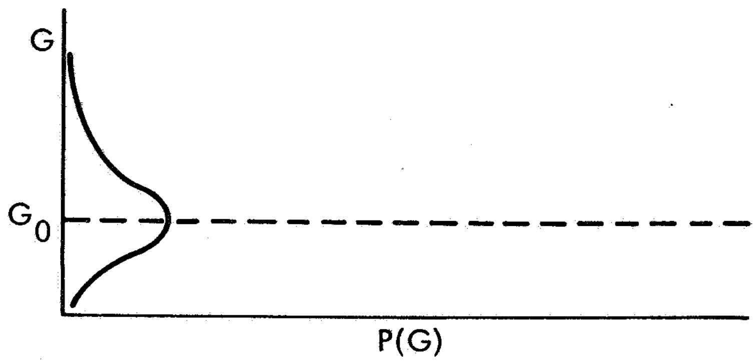


Figure II-5. Radiometer gain probability distribution.

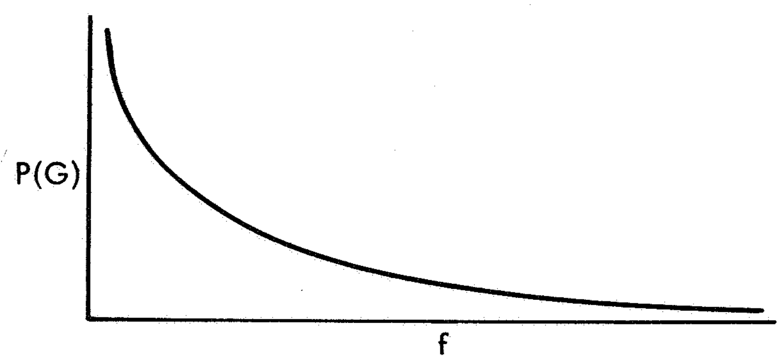


Figure II-6. Radiometer gain probability spectrum.

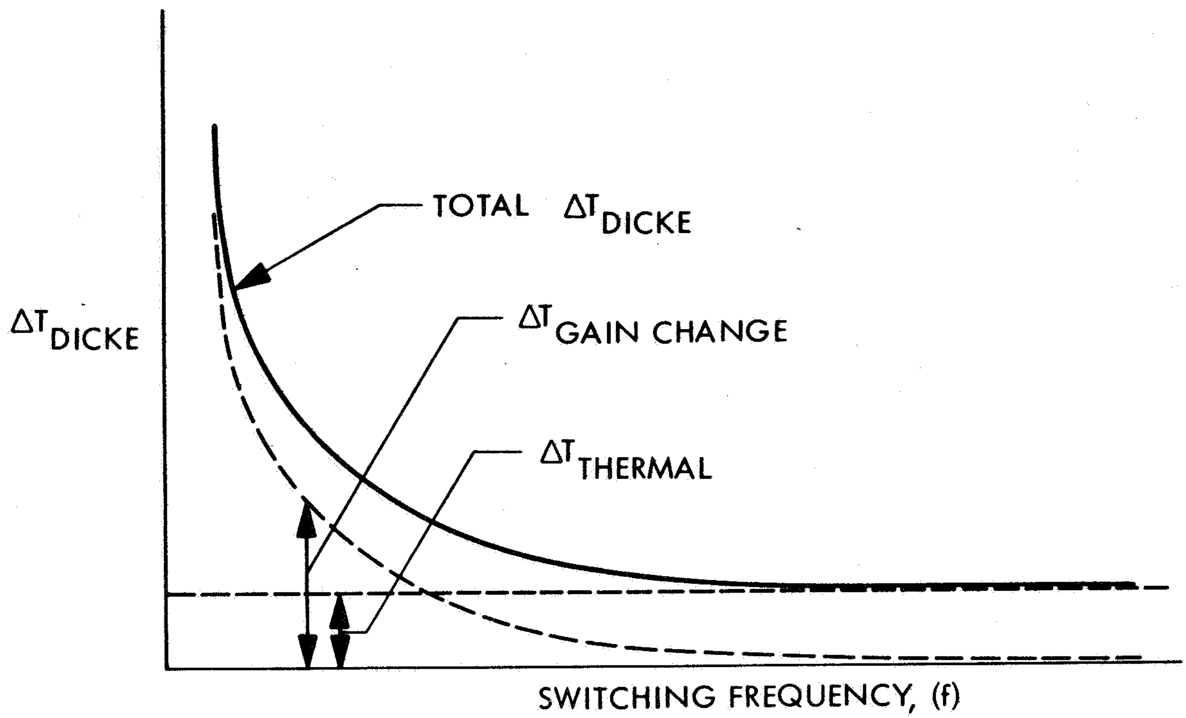


Figure II-7. Noise jitter vs. switching frequency for idealized Dicke radiometer.

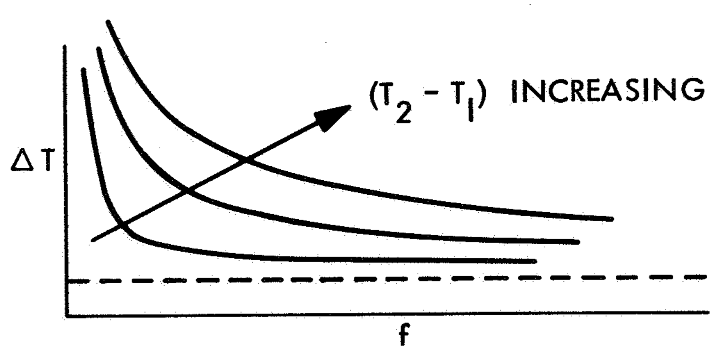


Figure II-8. $\Delta T$ vs. switching frequency for various values of $(T_2 - T_1)$.

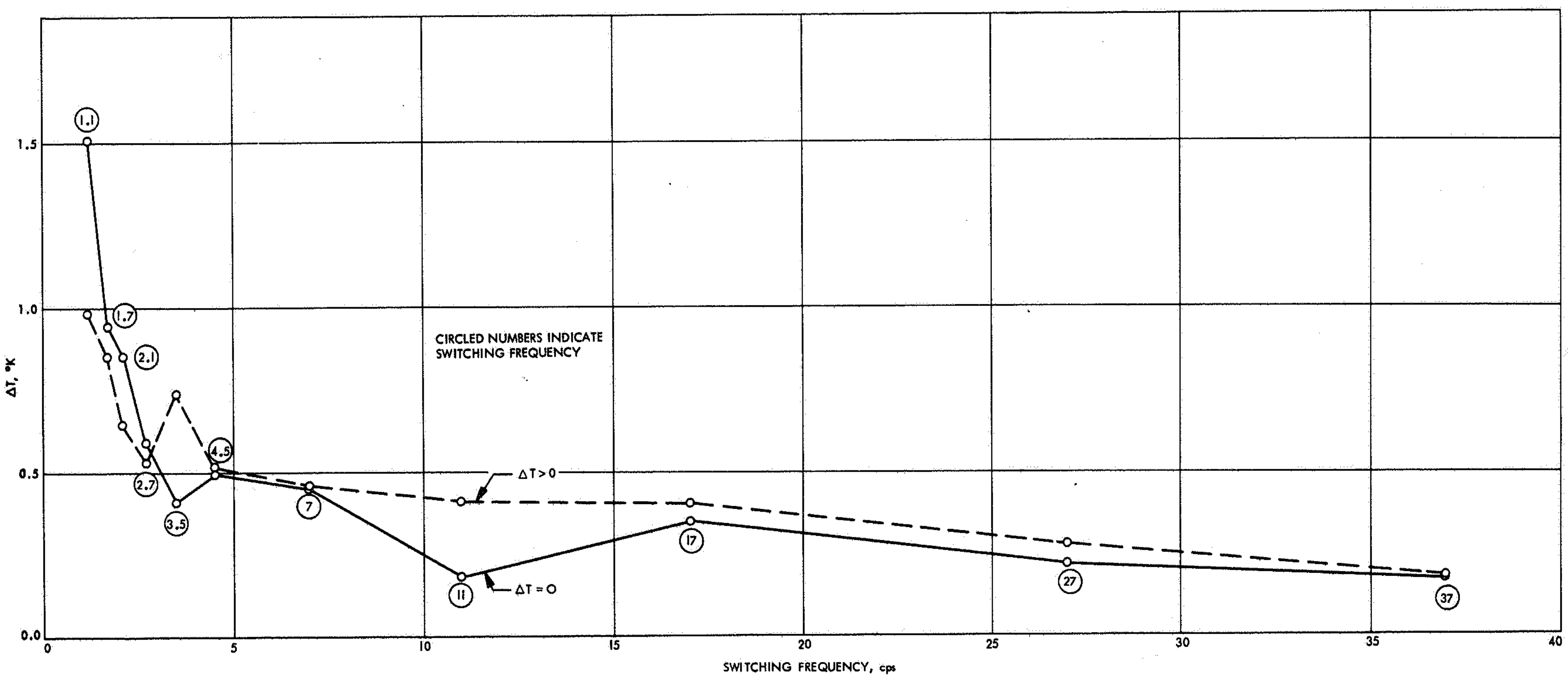


Figure II-9. Experimental results, $\Delta T$ vs. switching frequency.

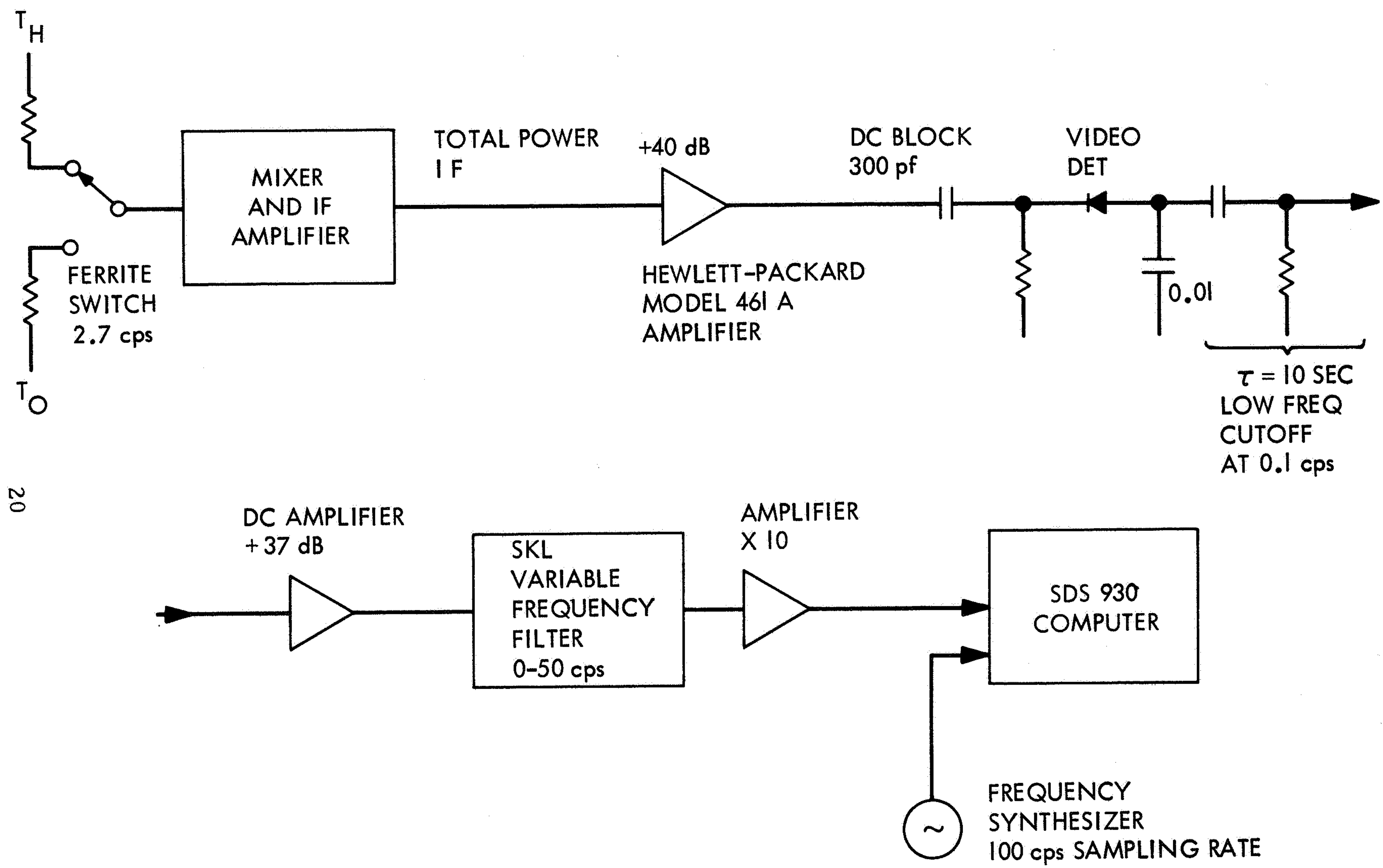


Figure II-10. Instrumentation for radiometer noise and gain change measurements.

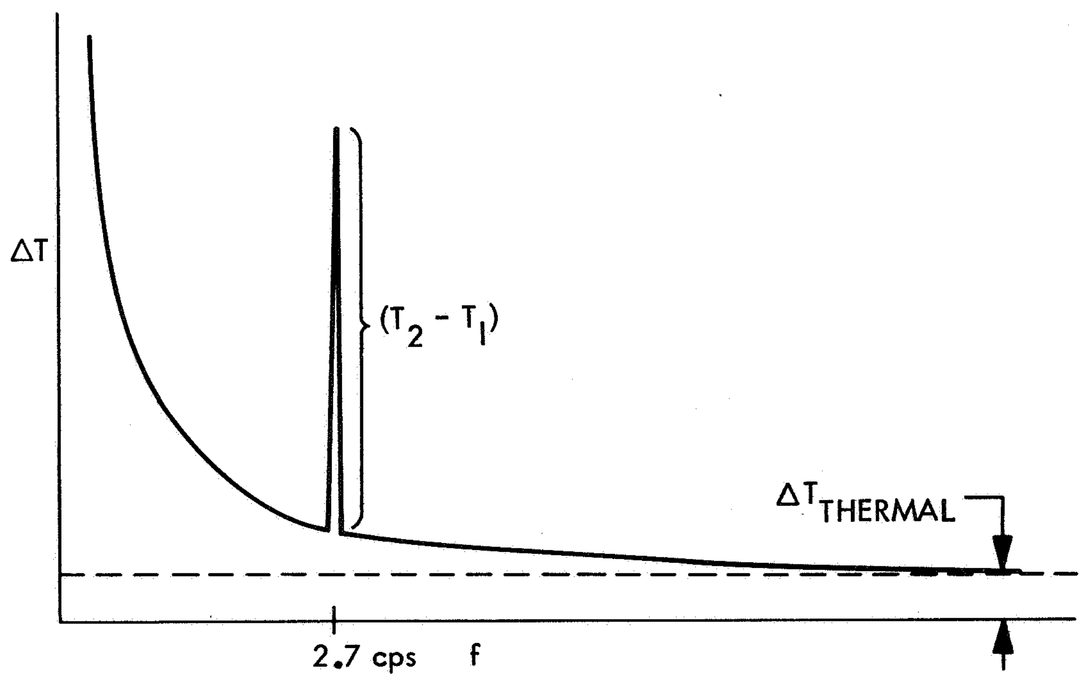


Figure II-11. Schematic spectral content of radiometer noise, with calibration pulse.

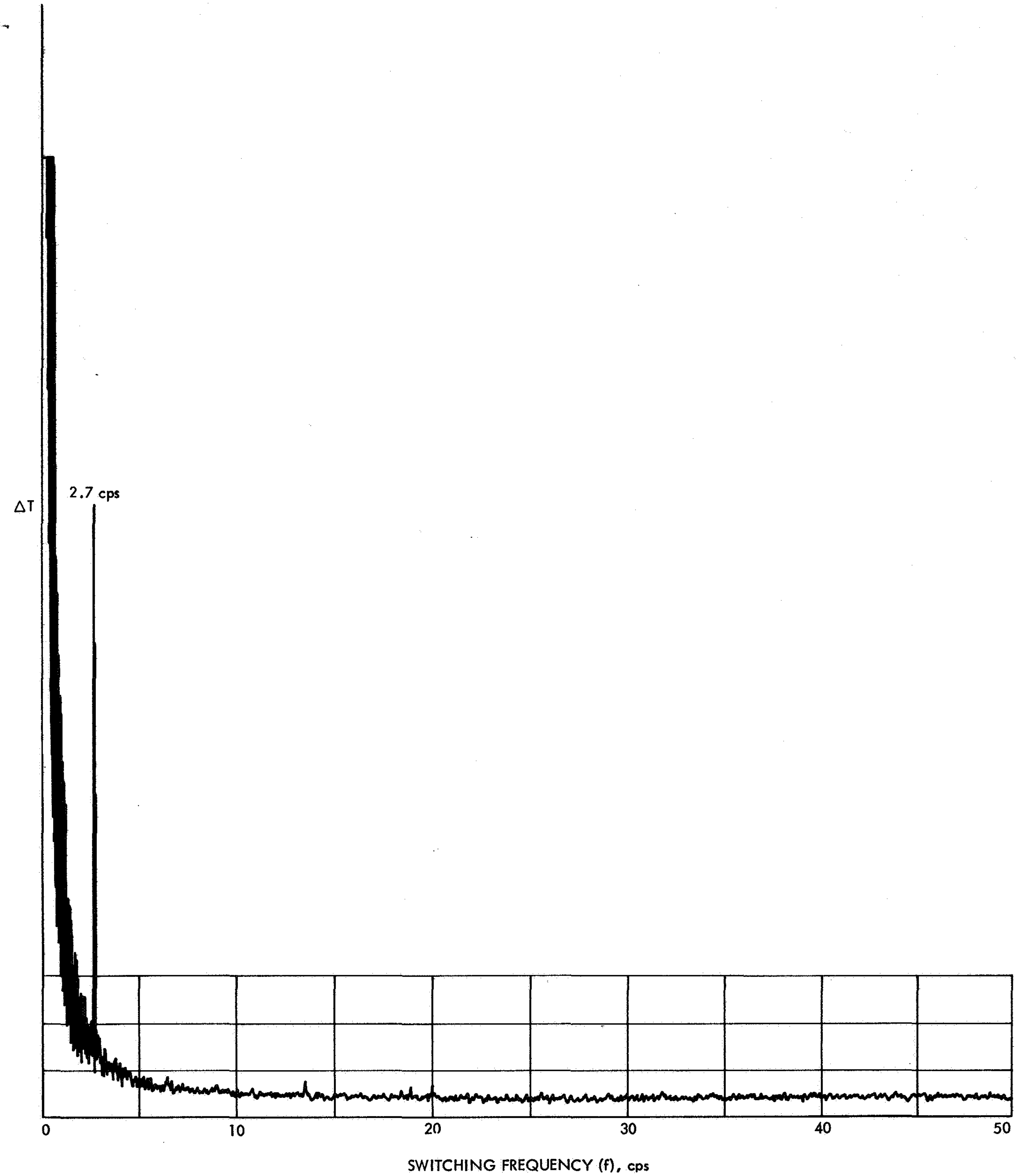


Figure II-12. Radiometer noise spectrum (0-50 cps)

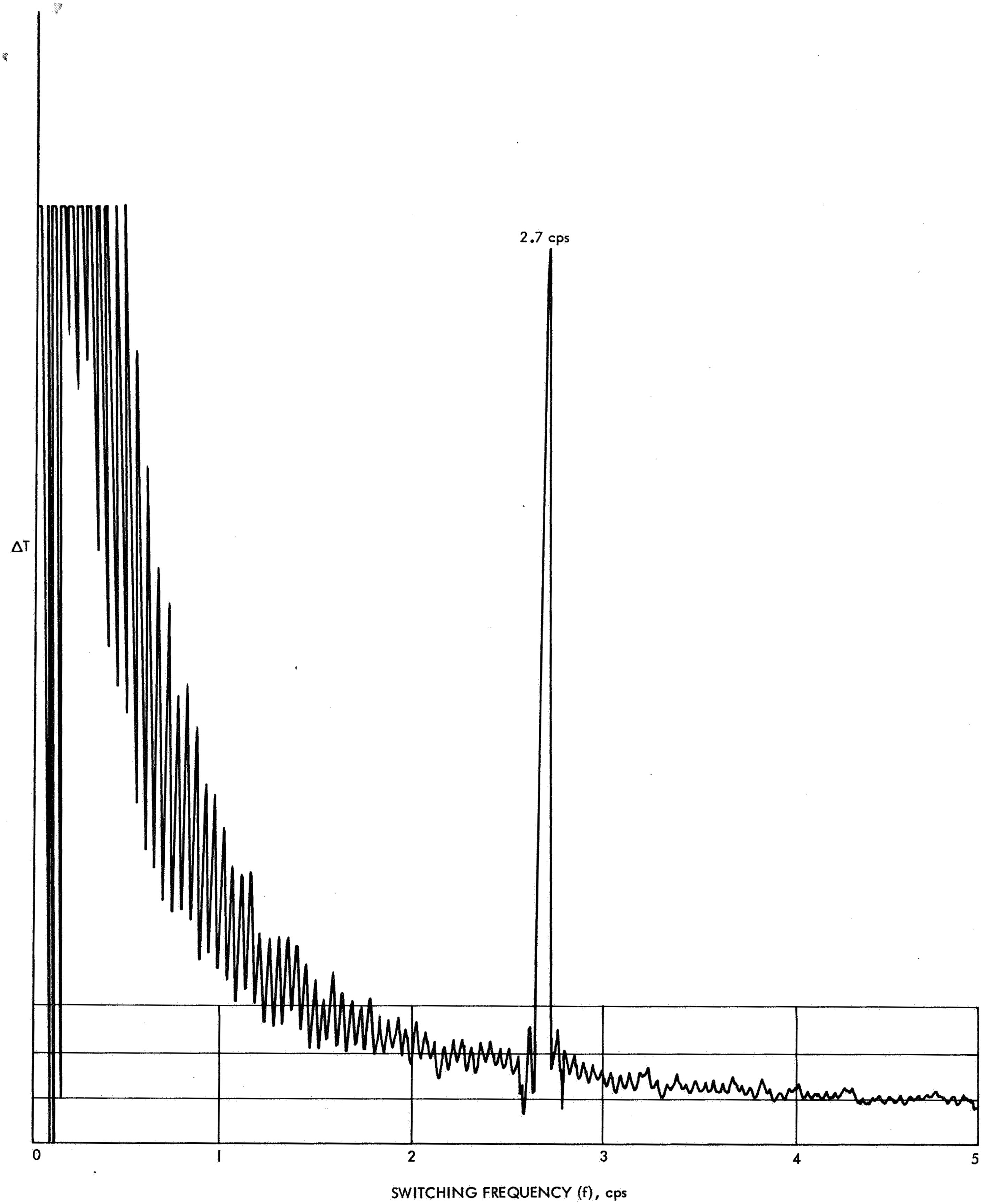


Figure II-13. Radiometer noise spectrum (0-5 cps)

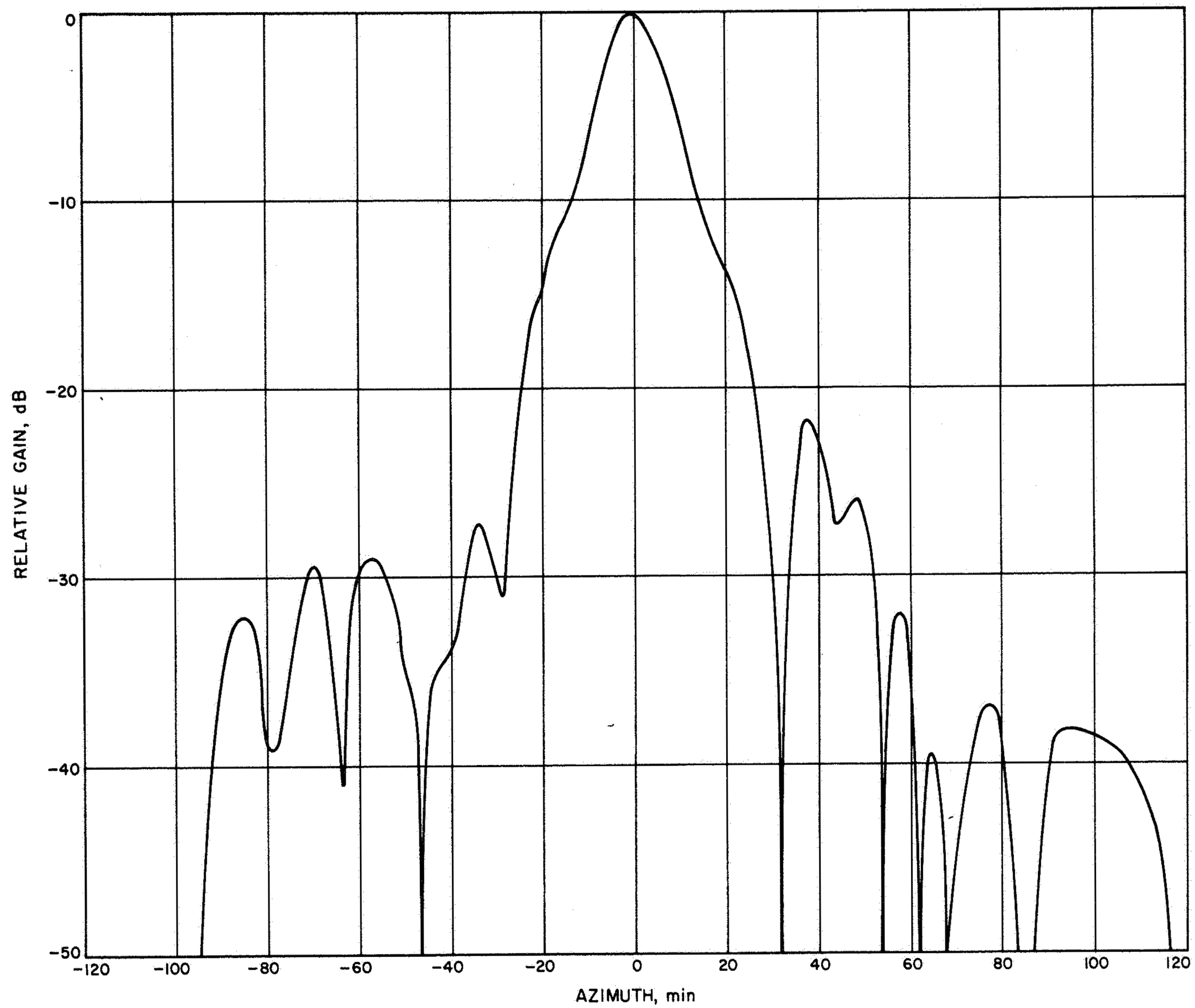


Figure II-14. Azimuth antenna pattern, tilted hyperboloid.

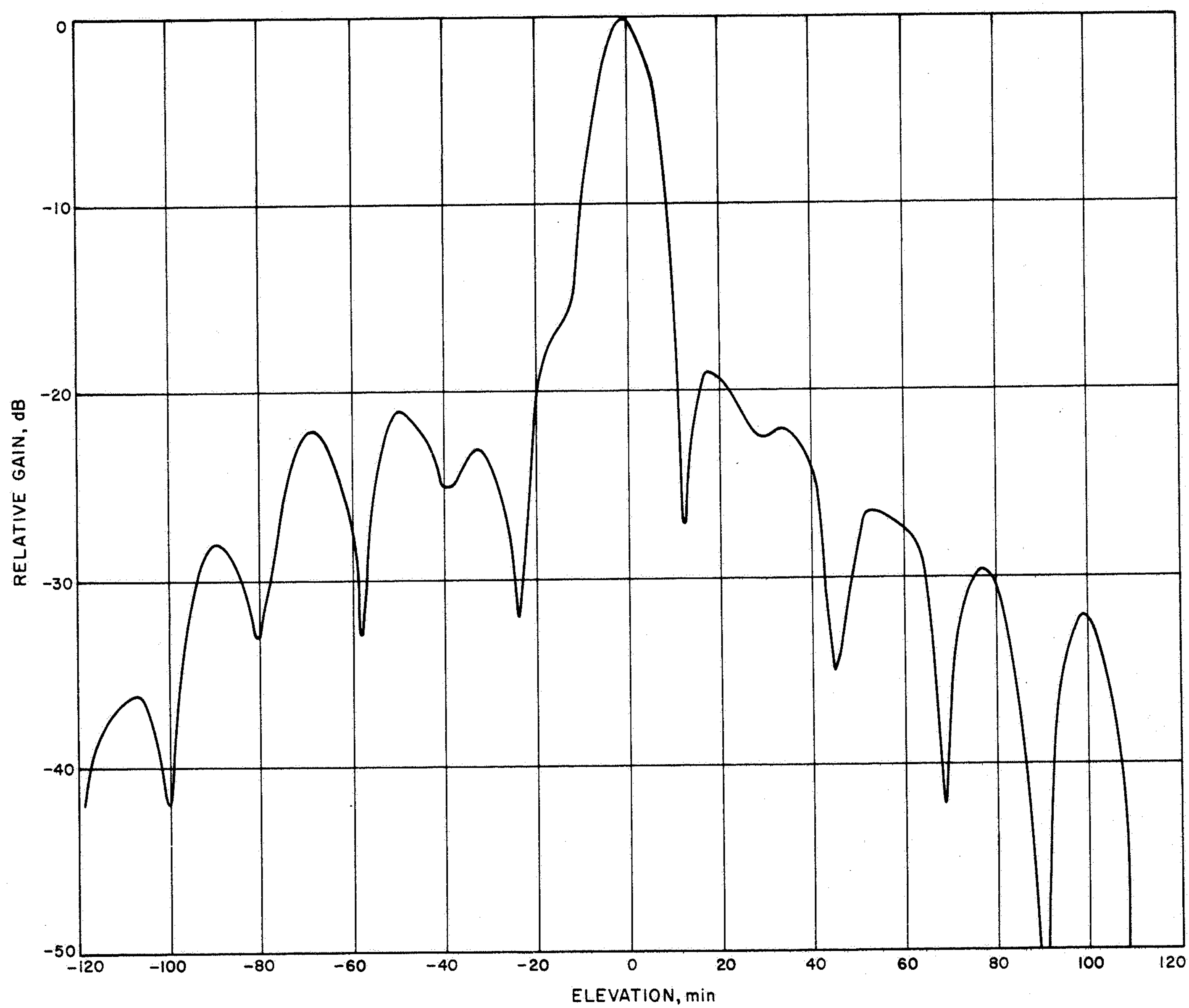


Figure II-15. Elevation antenna pattern, tilted hyperboloid.

## III. THEORY OF TILTED HYPERBOLOID

A. Analysis - Scattered Field for $\alpha = 2.06^\circ$. A preliminary description of the theoretical problem of scattering from an asymmetric hyperboloid was given in the last final report.[1] The geometry of the problem is shown in Figure III-1. The primary field emanates from 0 (in the $x_1, z_1$ system) in the form of a spherical wave and impinges on the tilted hyperboloid. The equations giving the scattered field at the field point P (in the $x_2 z_2$ system) are

$$E_\theta(P) = \frac{-j(kep)}{2\pi} \frac{e^{-jkR}}{R} \int_{\theta_0}^{\pi} \frac{\sin\theta_3}{(1 + e\cos\theta_3)^2} \cdot$$

$$\cdot \left[ \int_0^{2\pi} \frac{\rho_3}{\rho_1} A(\theta_1) M(\theta_3, \varphi_3) e^{-jk\rho_1} e^{jk\rho_2 [\sin\theta \sin\theta_2 \cos(\varphi-\varphi_2) + \cos\theta\cos\theta_2]} d\varphi_3 \right] d\theta_3 \tag{III-1}$$

$$E_\varphi(P) = \frac{-j(kep)}{2\pi} \frac{e^{-jkR}}{R} \int_{\theta_0}^{\pi} \frac{\sin\theta_3}{(1 + e\cos\theta_3)^2} \cdot$$

$$\cdot \left[ \int_0^{2\pi} \frac{\rho_3}{\rho_1} A(\theta_1) N(\theta_3, \varphi_3) e^{-jk\rho_1} e^{jk\rho_2 [\sin\theta \sin\theta_2 \cos(\varphi-\varphi_2) + \cos\theta\cos\theta_2]} d\varphi_3 \right] d\theta_3 \tag{III-2}$$

---

[1] Rusch, W. V. T., S. Slobin, and C. T. Stelzried, "Millimeter-Wave Radiometry for Radio Astronomy," Final Report, USCEE Report 183, University of Southern California, Los Angeles, December 1966, p. 7.

where $A(\theta_1)$ = primary source feed function

$M(\theta_3, \varphi_3)$ = (DH-EG) cos θ cos φ + (EF-CH) cos θ sin φ + (CG-DF) (-sin θ)

$N(\theta_3, \varphi_3)$ = (DH-EG) (-sin φ) + (EF-CH) cos φ

and $C(\theta_3, \varphi_3) = \cos\alpha(\sin\theta_3 \cos\varphi_3) - \sin\alpha(e + \cos\theta_3)$

$D(\theta_3, \varphi_3) = \sin\theta_3 \sin\varphi_3$

$E(\theta_3, \varphi_3) = \sin\alpha(\sin\theta_3 \cos\varphi_3) + \cos\alpha(e + \cos\theta_3)$

$F(\theta_1, \varphi_1) = (1 + \cos\theta_1) \sin\varphi_1 \cos\varphi_1$

$G(\theta_1, \varphi_1) = \cos\theta_1 \sin^2\varphi_1 - \cos^2\varphi_1$

$H(\theta_1, \varphi_1) = -\sin\theta_1 \sin\varphi_1$

$k\rho_1$, $k\rho_2$, $\theta_1$, $\varphi_1$, $\theta_2$, $\varphi_2$ are all related to $\theta_3$ and $\varphi_3$ through coordinate transformations

$E_\theta(P)$, $E_\varphi(P)$ are referred to the $x_2, z_2$ coordinate system.

The primary source feed function, $A(\theta_1)$, is given by the following expression:[2]

$$A(\theta_1) = \frac{\sin\left(\frac{\pi d}{\lambda\sqrt{2}} \sin\theta_1\right) \cos\left(\frac{\pi d}{\lambda\sqrt{2}} \sin\theta_1\right)}{\left(\frac{\pi d}{\lambda\sqrt{2}} \sin\theta_1\right)\left(1 - \frac{2d^2}{\lambda^2} \sin^2\theta_1\right)} \qquad \text{(III-3)}$$

where d = side dimension of diagaonal horn aperture

$\theta_1$ = angle measured in $x_1, z_1$ system

---

[2] A. W. Love, "The Diagonal Horn Antenna", <u>The Microwave Journal</u>, Vol. V, No. 3, pp. 117-122, March, 1962.

Feedhorn pattern measurements (cf. Section II-C) show that this theoretical expression is experimentally correct.

For the tilted hyperboloid system, with the tilt angle = $2.06^{\circ}$, a series of computer computations based on numerical integration of the above field equations was undertaken. Figure III-2 shows schematically the geometry and geometrical values upon which the computations are based. A computer listing of the complete FORTRAN IV computational program, including subroutines for calculating the phase of the scattered field and calculating the feed horn pattern is shown in Appendix A. A page of sample computer output, with pertinent answers, is shown in Figure III-3. Since each set of computations takes a great deal of computer time (approximately 1.3 minutes per field point), the calculations were broken up into groups of about 18 field points in order to limit computer time to less than one-half hour for each set.

Figure III-4 shows the results of the computer calculations of the field scattered from a tilted hyperboloid. Both the normally polarized and cross-polarized components of the scattered field are indicated. The normally polarized component has a small peak at $\theta = 356^{\circ}$. This may be interpreted as the position of expected specular reflection, and corresponds to the fact that in an optical situation the deviation of the light beam is twice the angular movement of the mirror. It can be seen from the figure that the scattered field retains its symmetrical characteristic, although it is displaced approximately $4^{\circ}$ from its symmetric position. Because of symmetry the only principal-plane cross-polarized field component is $E_\theta$ in the $\varphi = 90^\circ$ plane. This component, as plotted in the Figure, is at least 52 dB below the normally polarized component.

B. Phase Center Determination for $\alpha = 2.06^\circ$. The electric field scattered from the hyperboloid is given as

$$E_s \sim \frac{e^{-jkR}}{R} \left[ \mathrm{Re}\, E + j\, \mathrm{Im}\, E \right] = \qquad \text{(III-4)}$$

$$\frac{e^{-jkR}}{R} \cdot e^{+j\Phi(\theta)} = \qquad \text{(III-5)}$$

$$\frac{e^{-jkR}}{R} \left[ \cos \Phi(\theta) + j \sin \Phi(\theta) \right] \qquad \text{(III-6)}$$

where

$$\Phi(\theta) = \tan^{-1} \left( \frac{\mathrm{Im}\, E}{\mathrm{Re}\, E} \right) \qquad \text{(III-7)}$$

and, E = integral computed by tilted hyperboloid computer program.

Consider the geometry shown in Figure III-5. The problem of finding a new equivalent phase center is a problem of determining the point F' which is the center of concentric spheres upon which the scattered field has approximately constant phase, in a specific sense.

The computer program computes the phase of the scattered field as determined by Equation (III-7). If the scattered field is measured from F, then we may write for the scattered field at P,

$$E_s \sim \frac{e^{-jkR}}{R} \cdot e^{+j\Phi(\theta)} \qquad \text{(III-8)}$$

If the scattered field is measured from F', then the scattered field at P is

$$E_s \sim \frac{e^{-j(kr-c)}}{r} \tag{III-9}$$

where the surface r = constant is required to be a surface of constant or nearly constant phase.

However, since the field point P is independent of the coordinate system, then the phases measured in both systems must be equal. However, due to variations in $\Phi(\theta)$ a truly spherical equiphase surface centered at F' may not exist. Nevertheless, a point F' may be defined such that it yields the "best" nearly constant phase spheres in a least squares sense. Consequently, to determine the position of F'

$$\Delta = (\text{computed phase at P}) - (\text{phase on sphere of constant radius})$$

is minimized in a least squares sense. This difference is

$$\Delta = [kR - \Phi(\theta)] - [kr-c] \tag{III-10}$$

but, $R = r + a\cos(\psi - \theta)$ for $R,\ r >> a$.

Therefore,

$$[kr + ka\cos(\psi-\theta) - \Phi(\theta)] - [kr-c] = \Delta \tag{III-11}$$

and

$$c + ka\cos(\psi-\theta) - \Phi(\theta) = \Delta \tag{III-12}$$

Equation (III-12) must be solved for a, $\psi$, and c to minimize the variance of the differences between the computed phase at P and the phase on a surface of constant radius passing through P.

Since $\Phi(\theta)$ as a function of $\theta$ is known, there must exist some values of a and $\psi$ which will minimize the variance of $\Delta$. However, since the phase $\Phi(\theta)$ of the scattered field changes rapidly and monotonically, the best-fit phase center will be a function of the range of $\theta$ considered.[3]

For accurate comparison with experimental determination of phase center, the theoretical calculations should be made using only those values of $\theta$ which are experimentally significant, i.e., only those values which will "illuminate" the paraboloid with the scattered field. Since the paraboloid in the nodding subdish system subtends an angle of $60^\circ$ from center to edge as viewed from the focus, values of $\theta$ should be confined to that range.

Since the incident spherical wave illuminates the subreflector symmetrically in $\phi_1$, $E_i(+\phi_1) = E_i(-\phi_1)$, the phase center will move only in the plane of tilt, i.e., only in the plane $\phi_1 = 0, \pi$.

The computed phase $\Phi(\theta)$ is a series of discrete values as determined by a computer printout of $E_\theta$ vs. $\theta$. We must write this computed phase as $\Phi_i(\theta_i)$.

Thus, the equation to be solved becomes

$$c + ka \cos(\psi - \theta_i) = \Phi_i(\theta_i) = \Delta_i \qquad \text{(III-13)}$$

---

[3] W.V.T. Rusch, "Phase Error and Associated Cross-Polarization Effects in Cassegrainian-Fed Microwave Antennas, IEEE Transactions on Antennas and Propagation, Vol. AP-14, No. 3, May 1966, p. 267.

The variance of the difference between the theoretical curve $[c + ka \cos(\psi - \theta_i)]$ and the "experimental curve" $[\Phi_i(\theta_i)]$ is

$$\sigma^2 = \sum_{i=1}^{N} \Delta_i^2 = \sum_{i=1}^{N} [c + ka \cos(\psi-\theta_i) - \Phi_i(\theta_i)]^2 \tag{III-14}$$

The unknown $\psi$ must be "separated" from the term $\cos(\psi-\theta_i)$ in order to determine a solution for c, $\psi$, and a by minimizing $\sigma^2$ with respect to these variables. Utilizing the equality

$$\cos(\psi-\theta_i) = \cos\psi \cos\theta_i + \sin\psi \sin\theta_i$$

we obtain

$$\sigma^2 = \sum_{i=1}^{N} [c + ka \cos\psi \cos\theta_i + ka \sin\psi \sin\theta_i - \Phi(\theta_i)]^2 \tag{III-15}$$

Applying the minimization conditions

$$\begin{aligned} &(1) \quad \frac{\partial\sigma^2}{\partial c} = 0 \\ &(2) \quad \frac{\partial\sigma^2}{\partial(ka\cos\psi)} = 0 \\ &(3) \quad \frac{\partial\sigma^2}{\partial(ka\sin\psi)} = 0 \end{aligned} \tag{III-16}$$

we obtain three homogeneous equations which may be solved for c, $\psi$, and a.

Equation (III-15) does not take into consideration the fact that the scattered field does not have a constant amplitude for each value of $\theta_i$; hence a weighting factor must be introduced to give a more accurate phase center determination. A weight can be assigned to each particular value of "experimental" point, $\Phi_i(\theta_i)$, in direct proportion to the power level of the scattered field at each corresponding $\theta_i$. Thus, with weighting considered, the variance is expressed as

$$\sigma^2 = \sum_{i=1}^{N} \omega_i(\Delta_i)^2 \tag{III-17}$$

where $\omega_i$ are the weights for each value of phase.

Rewriting the variance relation in the form of equation (III-14), we obtain

$$\sigma^2 = \sum_{i=1}^{N} \omega_i \left[c + ka \cos(\psi-\theta_i) - \Phi_i(\theta_i)\right]^2$$

Applying the minimization conditions, we obtain

$$(1) \quad \sum_{i=1}^{N} 2\omega_i \left[c + ka \cos\psi \cos\theta_i + ka \sin\psi \sin\theta_i - \Phi_i(\theta_i)\right] = 0$$

$$(2) \quad \sum_{i=1}^{N} 2\omega_i \left[c + ka \cos\psi \cos\theta_i + ka \sin\psi \sin\theta_i - \Phi_i(\theta_i)\right]\left[\cos\theta_i\right] = 0$$

$$(3) \quad \sum_{i=1}^{N} 2\omega_i \left[c + ka \cos\psi \cos\theta_i + ka \sin\psi \sin\theta_i - \Phi_i(\theta_i)\right]\left[\sin\theta_i\right] = 0$$

(III-18)

Equations (III-18) have been solved for a range of $\theta_i$ of $\pm 60^\circ$. The solutions are:

$$a = 1.69\,\lambda$$
$$\psi = 87.938^\circ$$
$$c = -44.522$$

The significance of these solutions may be seen in Figure III-5. c represents the phase on a particular constant phase surface which best fits the input data. Figure III-6 compares the phase on spheres centered at both F and F'. The phase measured from the origin varies over more than $1100^{\circ}$, whereas the phase measured from the new phase center (as determined by a and $\psi$ above) varies by less than $70^{\circ}$. The curves do not show the discrete values of phase, but the trends are easily seen.

The position of the phase center determined by the cosine curve fitting method is different from the actual physical position of the focus of the hyperboloid in its tilted position. The new position of the hyperboloid focus is at

$$a = 0.705\,\lambda$$

$$\psi = 88.97^{\circ}$$

Thus, the computed phase center is almost one wavelength farther from F (cf. Figure III-5) than the new position of the hyperboloid focus.

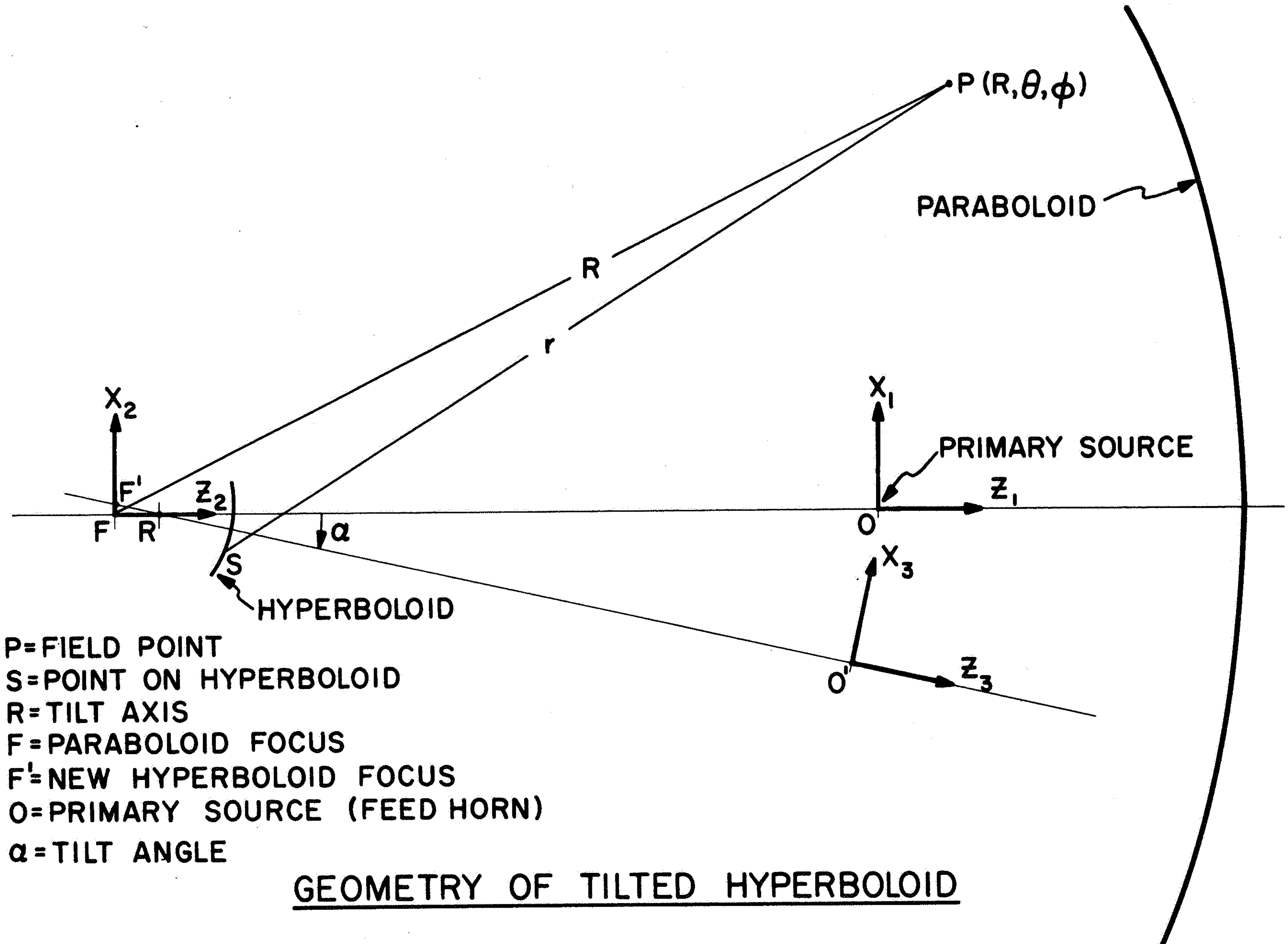

P (R,θ,φ)
PARABOLOID
R
r
X2
X1
PRIMARY SOURCE
F'
Z2
Z1
F
R
α
O
S
X3
HYPERBOLOID
O'
Z3
P=FIELD POINT
S=POINT ON HYPERBOLOID
R=TILT AXIS
F=PARABOLOID FOCUS
F'=NEW HYPERBOLOID FOCUS
O=PRIMARY SOURCE (FEED HORN)
α=TILT ANGLE
GEOMETRY OF TILTED HYPERBOLOID


Figure III-1.

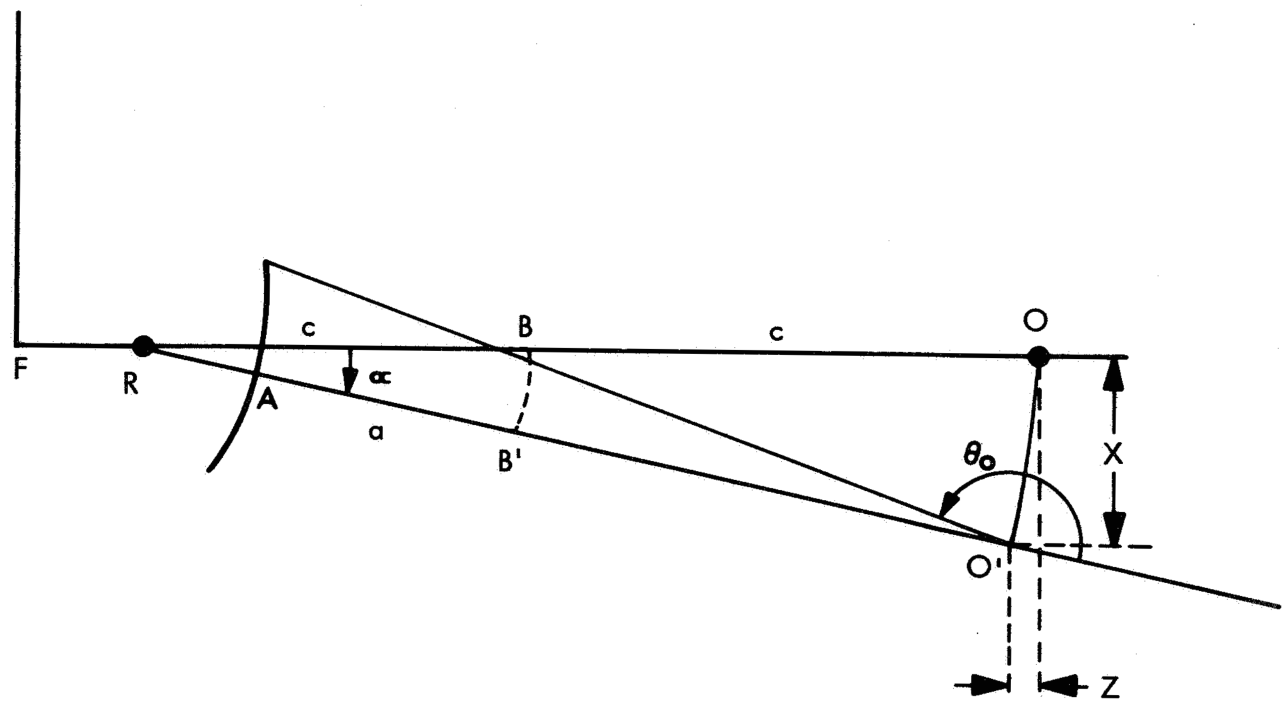


Radius of hyperboloid = 3.9000"
Distance between foci = FO = 2c = 25.600"
a = 9.63107" = AB'
c = 12.80000" = BO
e = c/a = 1.32903
RA = 0.600"
FA (untilted) = c-a = 3.16893"
depth of hyperboloid = 0.981"
$\alpha = 2.06^{\circ}$
X = 0.82762"
Z = 0.01488"
$\theta_o = 170.54^{\circ}$
$k = 2\pi/\lambda = 1886.26022$ meter$^{-1}$
$f = 90.0 \times 10^{9}$ cycles per second
O = symmetric focus
O' = tilted focus

Figure III-2. Schematic view of geometry and geometrical values.

ALPHA = 2.06 90 GC FORTRAN 4 COMPLETE RUN TILTED HYPER

INPUT PARAMETERS AND CONTROL CONSTANTS

| | | | | | | | |
|---|---|---|---|---|---|---|---|
| THETA= | 1.00000 DEGREES | INCREMENT= | 2.00000 | | | | |
| PHI= | 180.00000 DEGREES | INCREMENT= | 180.00000 | | | | |
| THETA(0)= | 170.53999 | KEP = | 353.60693 | E = | 1.32903 | ALPHA = | 2.06000 |
| KX = | 39.65221 | KZ = | 0.71282 | KOF = | 1226.52539 | | |

OUTER INTEGRAL STEP= 0.00129 RADIANS = 0.07391 DEGREES

PHI= 3.14159 RADIANS= 179.99994 DEGREES

| THETA | E THETA | | | | E PHI | | | |
|---|---|---|---|---|---|---|---|---|
| DEGREES | REAL | IMAGINARY | MAGNITUDE | PHASE | REAL | IMAGINARY | MAGNITUDE | PHASE |
| 1.000 | -0.00197988 | 0.00133791 | 0.00238954 | 145.951 | -0.00000000 | 0.00000000 | 0.00000000 | 141.234 |
| 3.000 | -0.00120721 | 0.00191923 | 0.00226733 | 122.170 | -0.00000000 | 0.00000000 | 0.00000000 | 133.489 |
| 5.000 | -0.00052201 | 0.00238776 | 0.00244418 | 102.332 | -0.00000000 | 0.00000000 | 0.00000000 | 143.583 |
| 7.000 | 0.00019978 | 0.00237676 | 0.00238714 | 85.199 | 0.00000000 | 0.00000000 | 0.00000000 | 82.440 |
| 9.000 | 0.00104162 | 0.00210458 | 0.00234824 | 63.668 | -0.00000000 | 0.00000000 | 0.00000000 | 100.628 |
| 11.000 | 0.00170666 | 0.00163680 | 0.00236470 | 43.803 | 0.00000000 | 0.00000000 | 0.00000000 | 71.294 |
| 13.000 | 0.00216801 | 0.00102863 | 0.00239966 | 25.382 | 0.00000000 | 0.00000000 | 0.00000000 | 35.780 |
| 15.000 | 0.00238972 | 0.00028931 | 0.00240717 | 6.903 | 0.00000000 | -0.00000000 | 0.00000000 | 350.350 |
| 17.000 | 0.00236280 | -0.00051155 | 0.00241754 | 347.784 | 0.00000000 | 0.00000000 | 0.00000000 | 8.515 |
| 19.000 | 0.00203103 | -0.00133604 | 0.00243107 | 326.662 | 0.00000000 | -0.00000000 | 0.00000000 | 315.686 |
| 21.000 | 0.00137970 | -0.00197617 | 0.00241179 | 304.894 | 0.00000000 | -0.00000000 | 0.00000000 | 288.596 |
| 23.000 | 0.00053225 | -0.00225615 | 0.00231808 | 283.274 | 0.00000000 | -0.00000000 | 0.00000000 | 280.621 |
| 25.000 | -0.00020320 | -0.00220124 | 0.00221060 | 264.726 | 0.00000000 | -0.00000000 | 0.00000000 | 284.290 |
| 27.000 | -0.00085166 | -0.00202701 | 0.00219866 | 247.210 | -0.00000000 | -0.00000000 | 0.00000000 | 252.977 |
| 29.000 | -0.00152240 | -0.00162732 | 0.00222842 | 226.908 | -0.00000000 | -0.00000000 | 0.00000000 | 206.643 |
| 31.000 | -0.00189039 | -0.00093947 | 0.00211096 | 206.426 | -0.00000000 | -0.00000000 | 0.00000000 | 208.081 |
| 33.000 | -0.00204414 | -0.00033213 | 0.00207095 | 189.229 | -0.00000000 | -0.00000000 | 0.00000000 | 181.410 |
| 35.000 | -0.00203331 | 0.00045011 | 0.00208254 | 167.518 | -0.00000000 | 0.00000000 | 0.00000000 | 147.993 |

IHC217I

| | | | |
|---|---|---|---|
| TRACEBACK FOLLOWS- | ROUTINE | ISN | REG. 14 |
| | IBCOM | | 8200E3C0 |
| | MAIN | | 00005FA8 |

ENTRY POINT= 50000820

Figure III-3. Sample computer output, tilted hyperboloid scattering.

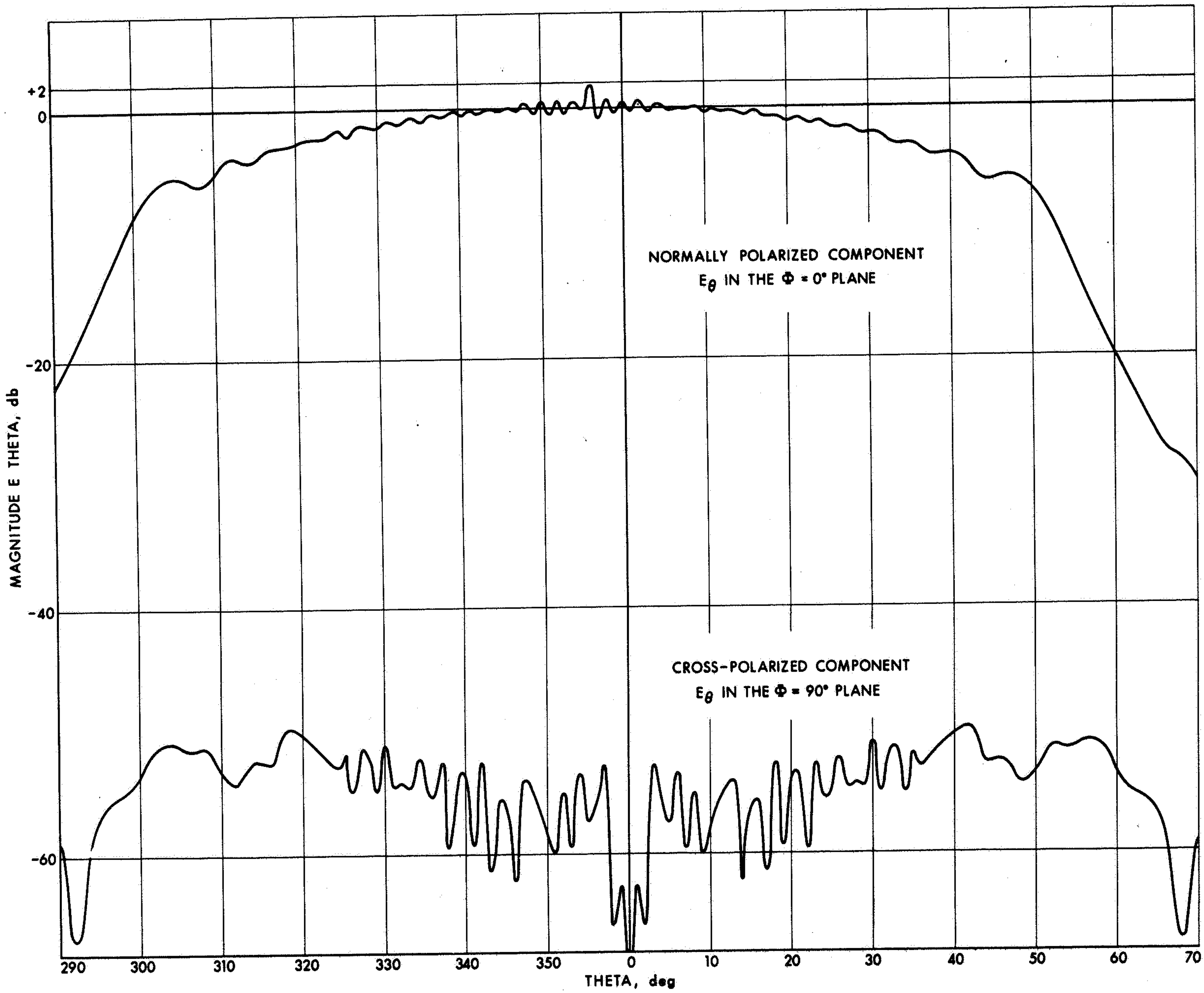


Figure III-4. Scattered field and cross-polarization patterns.

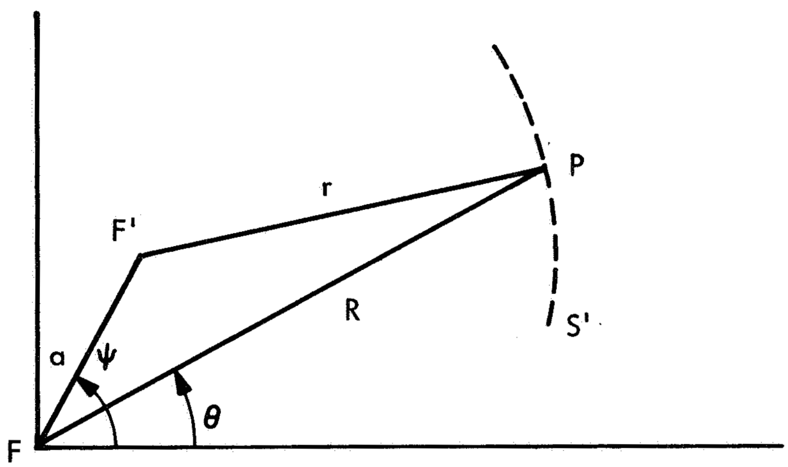


Figure III-5. Phase center geometry, tilted hyperboloid.

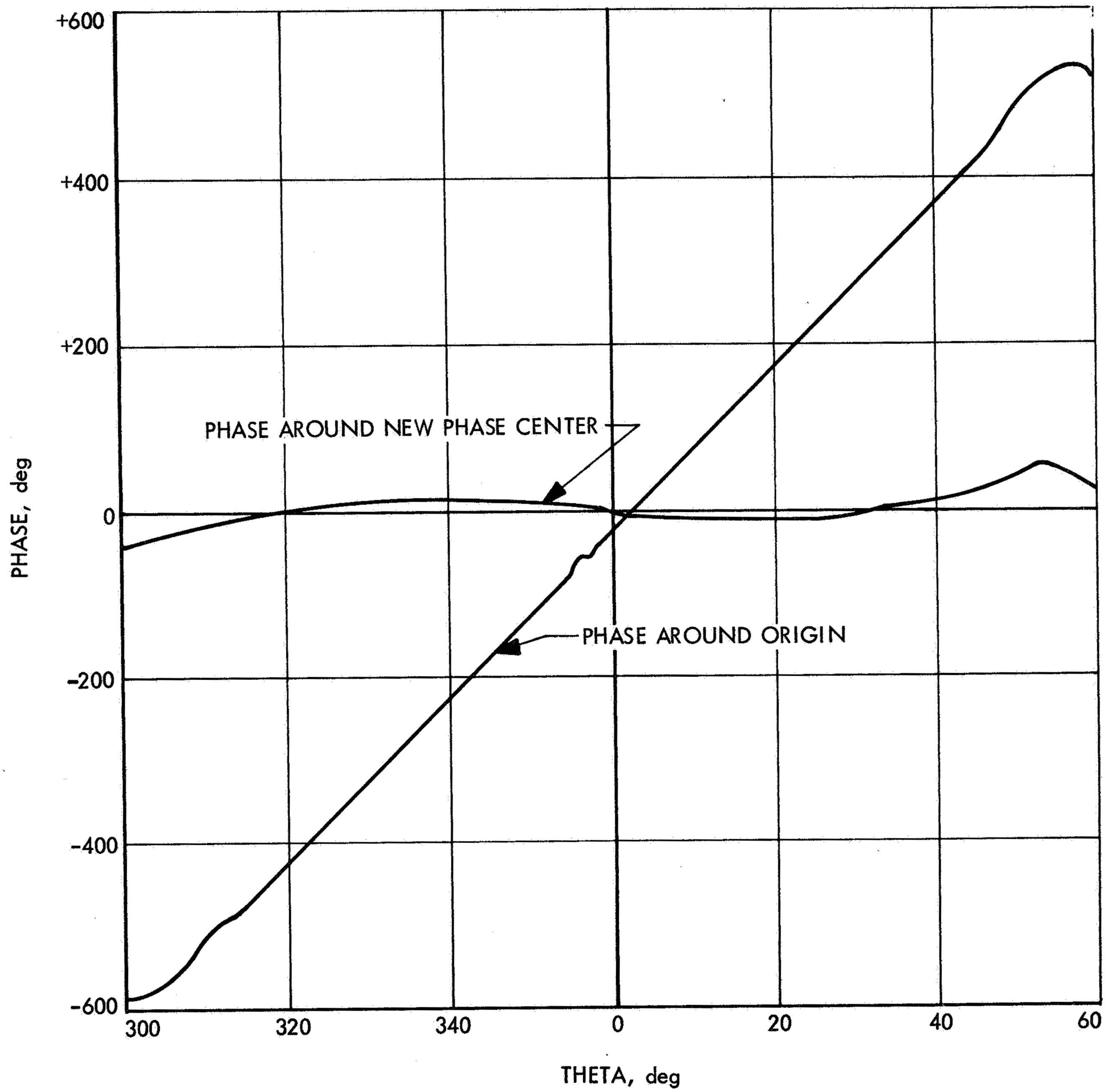


Figure III-6. Computed phase on spheres of constant radius around origin and around new phase center.

## IV. LUNAR ECLIPSE OF 18 OCTOBER 1967

Radiometric observations of a total lunar eclipse were carried out on 18 October 1967 from the Venus site at the Goldstone Tracking Station in the Mojave Desert (Fig. IV-1). Operational details of the antenna and radiometer are described in Section II. The center of the moon was tracked optically with a 40-power sighting telescope which had been aligned with the primary antenna beam. The NSS then directed the reference antenna beam to a position in the sky 55. 5 arcminutes in declination above the primary beam. (The measured isolation between these two beams was 33 dB.) Seventy-one observations of the center of the moon were made from 0207 to 1315 on 18 October (UT).

During the 16 observations prior to local midnight, a relatively low-data-rate observing sequence was used for the purpose of calibrating the system and, at the same time, obtaining atmospheric information. This low-data-rate sequence consisted of the following steps:

1. The center of the moon was tracked for 120 seconds during which time the antenna switched at a rate of 2.7 cps between the moon (primary beam) and the sky (reference beam).

2. The waveguide switch was rotated to the calibration path (cf. Fig. II-1). A reference signal was obtained for 120 seconds from the output port of a switching circulator which switched alternately between heated and ambient terminations, the temperatures of which were monitored continuously by a

quartz thermometer and displayed digitally in the radiometer control room. (During this period the antenna continued to track the moon as in Step 1.)

3. The waveguide switch was returned to its original position in the rf path. The antenna continued to track the moon as in Step 1; however, the subdish drive mechanism was deactivated for 60 seconds so that a reference signal was no longer available for the radiometer (cf. Fig. II-3). The resulting "zero" radiometer output corresponded to the radiometer switching between two equal inputs (assuming ideal radiometer performance). This reference output will be subsequently referred to as the "electronic" baseline.

4. The subdish drive mechanism was reactivated, causing a reference signal to be transmitted to the radiometer. The NSS and radiometer then operated in the normal mode of operation. However, for the first time the antenna drive was turned off, allowing the earth's rotation to displace the antenna beam two degrees east of the moon. By this time the NSS was switching between two nearly equal-temperature positions in the sky, and the zero-output radiometer reference thus obtained (subsequently referred to as the "sky" baseline) was measured for an additional 120 seconds.

During the 55 observations made after local midnight a relatively high data-rate observing sequence was used, because the lunar eclipse took place during this period. This high-data-rate sequence consisted of the following two steps:

1'. Same as Step 1.

2'. Same as Step 3.

Every fourth two-step cycle of this type was followed by a more extended four-step calibration sequence consisting of:

1". Same as Step 1.

2". Same as Step 3.

3". Same as Step 2.

4". Same as Step 4.

The data were recorded on a strip-chart recorder with a radiomater post-detection time constant of three seconds. Sample chart recordings of runs 6D to 10D are shown in Figure IV-2. The data were also recorded on a digital counter-printer, with effective counting intervals of 60 seconds for the electronic baseline and 120 seconds for the moon, calibration, and sky baseline. These digital results, with the computed probable errors, are tabulated in the Appendices. The digital results corresponding to the strip-chart record of runs 6D to 10D indicated in Figure IV-2 were converted into equivalent antenna temperature (referred to the aperture of the antenna). The average probable error of each moon-track, calibration, and sky-baseline data point was $0.36^{\circ}K$. (This value is proportional to the jitter of the pen recording in Figure IV-2.) The average probable error of the electronic-baseline data was $0.05^{o}K$.

A. Gain Calibration. The data obtained during Step 2 of the low-data-rate sequence and Step 3'' of the high-data-rate sequence provided a means to monitor the relative system gain during the experiment. In this mode of operation an amount of power proportional to the known temperature differences between the heated and ambient terminations was injected into the radiometer, i.e., $P_i = C(T_h - T_a)$, where the constant C is determined by various physical constants and such system constants as the insertion loss between the heated termination and the reference point at the output of the waveguide switch. If the radiometer output voltage is assumed to be linearly related to the power injected into the RF path, then the radiomater gain will be given by

$$G_{rad} = \frac{V_{cal} - V_{baseline}}{C(T_h - T_a)} \qquad (IV-1)$$

where $V_{cal}$ is the output voltage during the calibration step and $V_{baseline}$ is the output voltage during the baseline step. (Unless specified otherwise the electronic baseline was used.)

Conversely, a system "transfer constant" may be defined by

$$STC = \frac{1}{GC} = \frac{(T_h - T_a)}{V_{cal} - V_{baseline}} \qquad (IV-2)$$

and the units of STC are degrees temperature difference (at the point of the heated termination) per voltage change at the radiometer output. Ultimately it is necessary to convert the STC to a temperature change at the reference point of the waveguide switch. However, the STC as defined above provides a convenient measure of the relative gain stability of the radiometer. Consequently, the 22 values of the system transfer constant measured during the night of the eclipse are plotted in Figure IV-3 as a function of Universal Time.

Superimposed on the data points in Figure IV-3 is a second-order curve fitted to the data. The jitter of the actual data with respect to this curve corresponds to gain changes of about 0.1 dB, while the long-term change over a period of nine hours corresponds to a gain drift of about 0.3 dB. This second-order curve fitted to the actual data points was used to normalize the moon-temperature data and thereby remove the effects of gain drift from the data.

B. Extinction Curve. A standard extinction curve of the data taken on 18 October is plotted in Figure IV-4. The ordinate is the logarithm of the STC-normalized antenna temperature, and the abscissa is the air mass calculated for an atmospheric scale height of 15 kilometers. For a constant source temperature and a constant atmospheric loss, the slope of an extinction curve of this type provides a direct measure of the atmospheric loss, and the intercept with the ordinate-axis is proportional to the source temperature.

Each pre-meridian-transit data point is plotted as a **dot** (•) in the figure. Since these observations were made prior to the eclipse, the brightness temperature of the moon may be presumed to have remained constant in this four-hour interval, and the data may be used to evaluate the atmospheric loss. Using a linearized curve-fitting procedure developed by Stelzried and Rusch[1], the loss before meridian transit was determined to be 0.36 dB with a probable error of 0.03 dB.

Each post-meridian-transit point is plotted in the figure with a circle (o). Also indicated are the approximate times for the beginning and ending of the umbral stage of the eclipse, and the beginning and ending of totality. The data are considerably compressed during the initial stage of the eclipse, because of the non-linear scales in a plot of this type. However, the effect of a changing source temperature is evident.

C. <u>Data Reduction.</u> $T_{AM}$, the equivalent antenna temperature of the moon (without atmospheric loss) is related to $T_A$, the measured antenna temperature relative to the aperture by

$$T_A = T_{AM}(L_O)^{-AM(Z)} \qquad \text{(IV-3)}$$

where Z is the zenith angle, AM(Z) is the equivalent air mass at each zenith angle, and $L_O$ is the atmospheric loss at zenith, i.e., unity air mass. If $L_O$ is known or assumed to be known, the relation can be inverted to yield the equivalent moon antenna temperature for each data point, i.e.,

---

[1] C. T. Stelzried and W. V. T. Rusch, "Improved Determination of Atmospheric Opacity from Radio Astronomy Measurements," Jour. Geophys. Res., Vol. 72, No. 9, May 1, 1967.

$$T_{AM} = T_A(L_O)^{+AM(Z)} \qquad \text{(IV-4)}$$

Assuming the pre-transit value of $L_O$ = 0.36 dB remained constant during the entire night of the eclipse, an equivalent moon antenna temperature can be determined for each of the 71 data points. These values, normalized to the average of the 13 pre-transit values, are plotted in Figure IV-5 as a function of universal time on 18 October. Also indicated are (A) the beginning of the umbral stage at 0826, (B) the beginning of totality at 0945, (C) the end of totality at 1046, and (D) the end of the umbral stage at 1205. A seven percent decrease in the lunar equivalent disc brightness temperature is evident.

The moon was too low in the sky to obtain the necessary post-eclipse data points necessary to establish an adequate secondary baseline. Consequently, there is some question about the proper value of $L_O$ to use for the post-transit data. The large zenith angles for the post-eclipse data points magnified loss-dependent effects. If the moon is assumed to have re-attained temperature equilibrium in the final few data points, a value of $L_O$ = 0.386 dB must be assumed. This value is within the probable error of the pre-transit value of 0.36 dB, indicating that it may be academic to attempt to refine the value of $L_O$ still further. Nevertheless, the data were replotted in Figure IV-6 using the value of $L_O$ = 0.386. The curve is virtually identical to Figure IV-5, except for the last few points. In either case the umbral cooling rates are the same and the maximum percentage temperature change is seven percent.

D. Conclusions.

1. A decrease of seven percent in the equivalent black-body disc temperature of the moon was measured during the total lunar eclipse of 18 October 1967. (The peak error estimated from Figures IV-5 and IV-6 is $\pm$ 0.5 percent.) If it is assumed that the equivalent black-body disc temperature of the full moon is 260°K at the measurement frequency of 90 GHz[2], this seven percent decrease amounts to a temperature decrease of about 18°K.

2. Using the value of 260°K to establish a full-moon equivalent disc-temperature calibration constant, the eclipse curves of Figures IV-5 and IV-6 indicate a cooling rate of about five degrees per hour during the umbral stage of the eclipse.

3. The measured jitter of the data points plotted in Figures IV-5 and IV-6 is 1.7 times as large as predicted by the measured short-term radiometer jitter. The fact that this jitter is larger than the theoretical value is due to (1) long-term radiometer fluctuations and/or (2) atmospheric scintillations and opacity fluctuations. Although additional quantitative data are presently unavailable, it is felt that the NSS has significantly reduced the atmospheric effects. A further evaluation of the atmospheric "smoothing" produced by the NSS is a significant area for additional investigation.

---

[2] Rusch, W. V. T., S. D. Slobin, and C. T. Stelzried, "Millimeter-Wave Radiometry for Radio Astronomy," Final Report, USCEE Rept. 183, University of Southern California, Los Angeles, December 1966, pp. 23-24.

E. Post-Eclipse Observations and Calibrations on 19 October.

Thirty-three observations of the moon were carried out on 19 October 1967, the night following the eclipse, using the low-data-rate sequence described earlier. The data from these observations, tabulated in the Appendices, served to further calibrate the system and evaluate its performance. The pre-transit and post-transit lunar extinction curves for 19 October are plotted in Figure IV-7. In this figure the pre-transit data points are indicated by dots (•) and the post-transit points by circles (o). The solid curves in the figure were fitted to the data points using the Stelzried-Rusch technique described earlier. The data in Figure IV-7 indicate that the atmospheric loss was changing during the seven-hour-long observations.

The observational data from 19 October provided a means to compare the two different baselines: the electronic baseline obtained by deactivating the subdish drive mechanism so that a reference signal was not available for the radiometer, and the sky baseline obtained by switching the NSS between two nearly equal-temperature positions in the sky. Prior to this point in the text all data was reduced using the electronic baseline. However, the low-data-rate sequence used on 19 October enabled both types of baseline to be determined in each of the 33 observation cycles.

Comparison of the two baselines is carried out in Table IV-1. In the left-hand column are the results of the data reduced using the electronic baseline for (1) the pre-meridian-transit data on 19 October, (2) the post-meridian-transit data on 19 October, and, as a reference, (3) the pre-meridian transit data on 18 October. The two quantities tabulated are

| | Electronic Baseline Data Reduction | Sky Baseline Data Reduction |
|---|---|---|
| Pre-Transit Data 19 October | $T_E = 213.1 \pm 1.4^{o}K$<br>$L_O = .261 \pm .019$ dB | $T_E = 211.1 \pm 1.3^{o}K$<br>$L_O = .247 \pm .017$ dB |
| Post-Transit Data 19 October | $T_E = 212.2 \pm 1.0^{o}K$<br>$L_O = .376 \pm .012$ dB | $T_E = 211.8 \pm 1.0^{o}K$<br>$L_O = .394 \pm .012$ dB |
| Pre-Transit Data 18 October | $T_E = 215.0 \pm 2.0^{o}K$<br>$L_O = .363 \pm .030$ dB | Not available |

TABLE IV-1

$T_E$, a hypothetical antenna temperature of the moon extrapolated above the atmosphere but not including certain calibration constants, and $L_O$, the atmospheric loss. It will be seen that $T_E$ remained essentially unchanged for the three sets of data. The two values of $L_O$ for 19 October were considerably different, indicating a changing atmosphere. In the right-hand column are the results of the data reduced using the sky baseline for the two periods on 19 October. The corresponding values of $T_E$ using the two techniques did not differ by more than a percent, and the corresponding values of $L_O$ did not differ by more than .02 dB. Although the measured differences in $T_E$ were within the overlapping probable errors, it was noticed that generally the sky baseline yielded a slightly lower extrapolated moon temperature than the electronic technique. This effect may have been due to either non-ideal radiometer performance or unequal antenna temperatures seen by the primary and reference beams after the antenna had drifted two degrees east of the moon. Whatever the cause, however, the data in Table IV-1 indicate that this effect introduced a possible error in the lunar equivalent disc temperature of no more than one percent.

A second procedure was carried out to evaluate the relative effects of the two different baselines. The data from 18 October were reduced in exactly the same manner described previously with the one exception that the sky baseline was used instead of the electronic baseline. Since sky-baseline information was obtained less frequently, fewer data points could be obtained in this manner. The resulting equilibrium moon temperature was less than one percent less. A normalized eclipse curve, such as the curve plotted in Figure IV-6, proved to literally overlay the curve derived using the electronic baseline. To indicate the similarity, the data from Figure IV-6 are reproduced identically in Figure IV-8 as circles (o). The normalized data using the sky baseline are superimposed on Figure IV-8 using solid dots. To within the scatter of the data points the two sets of data are identical. Consequently, the conclusions stated in the previous section about the eclipse results appear to be valid for data reduced using either type of baseline.

Figure IV-1. 90-GHz radio telescope at JPL Goldstone Tracking Station (control trailer and 30-ft antenna in background).

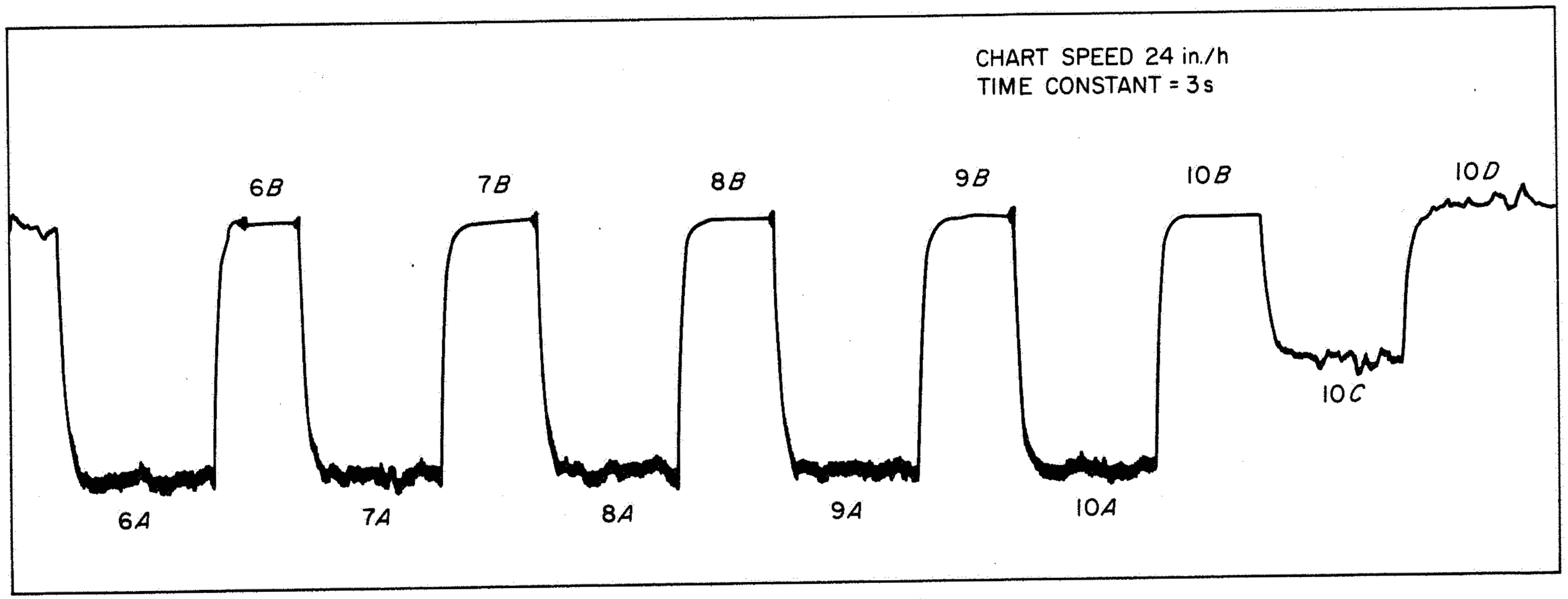


Figure IV-2. Strip chart recording during lunar eclipse measurements (A=moon, B=electronic baseline, C=hot load, D=sky baseline).

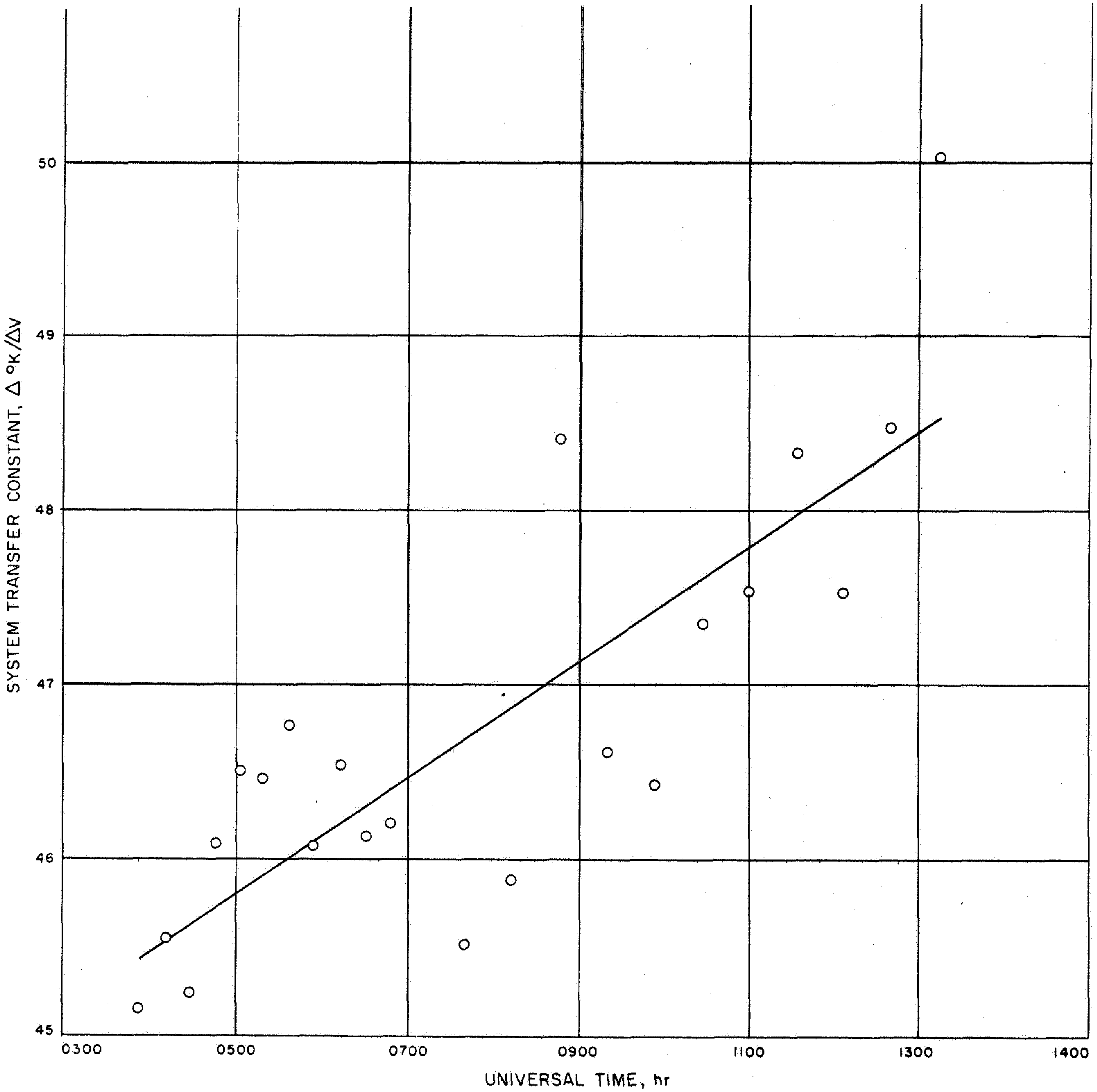


Figure IV-3. System transfer constant during night of eclipse (18 October 1967).

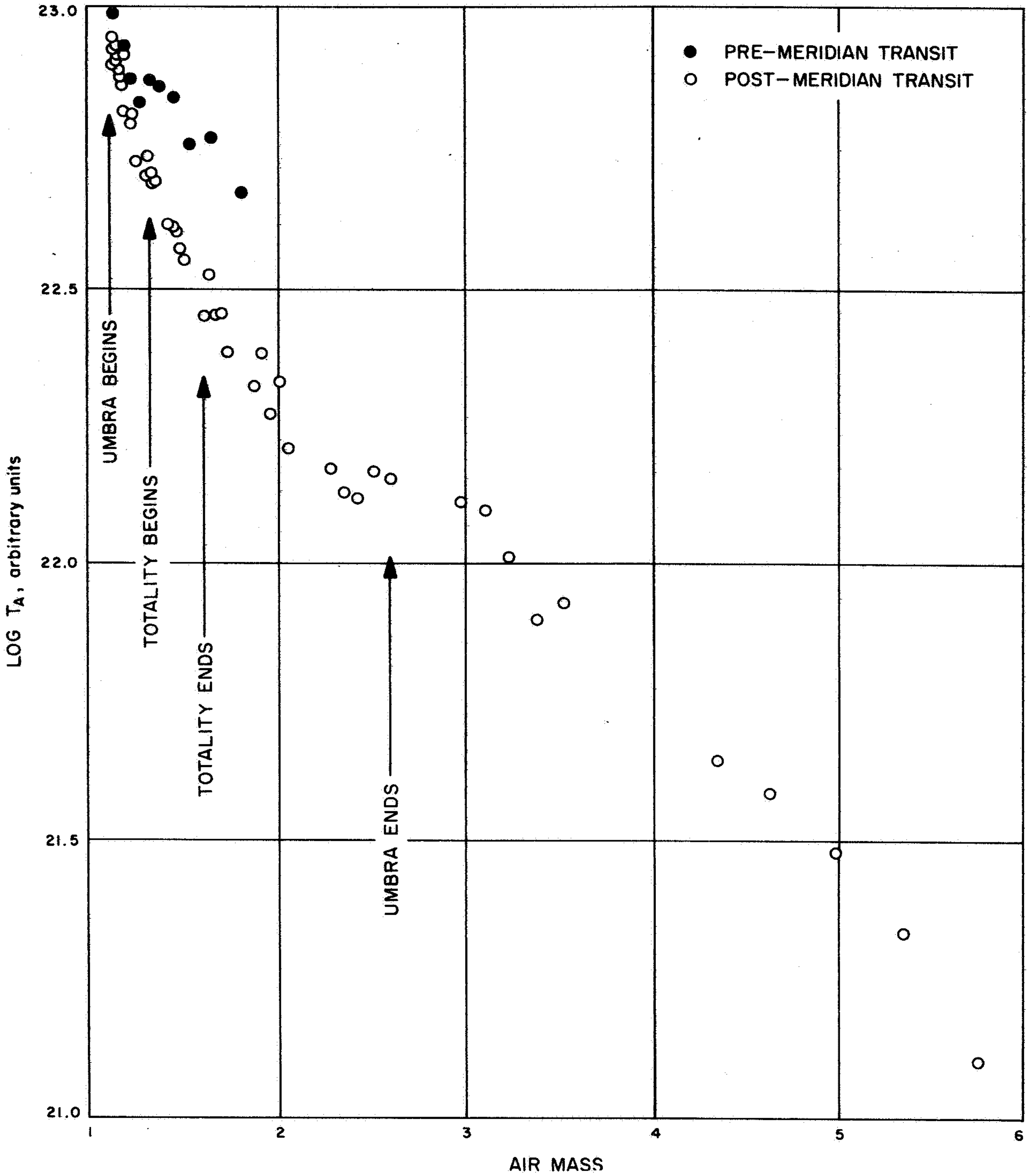


Figure IV-4. Lunar extinction curve during night of eclipse.

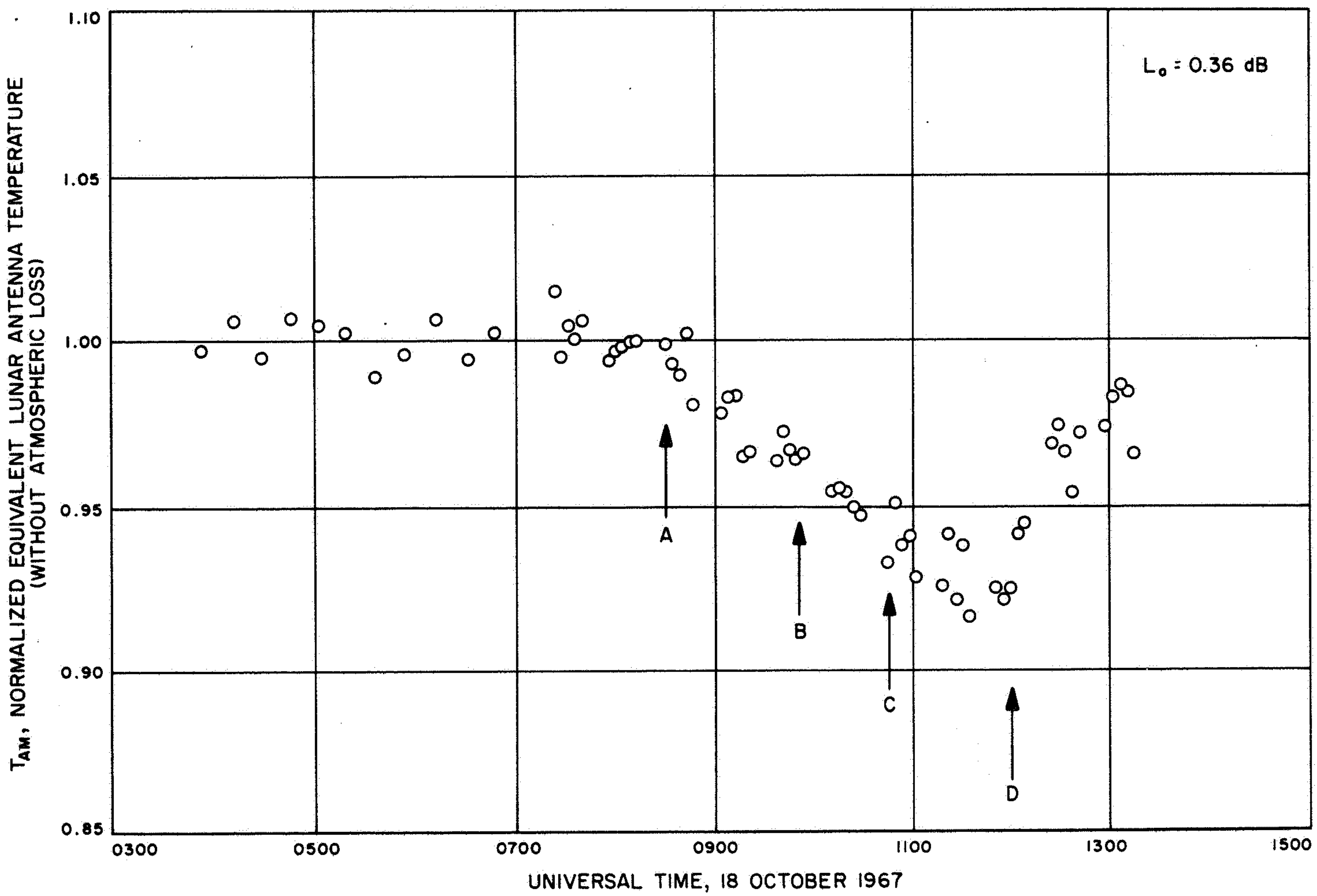


Figure IV-5. Equivalent lunar antenna temperature during night of eclipse, using electronic baseline ($L_o$ = 0.36 dB).

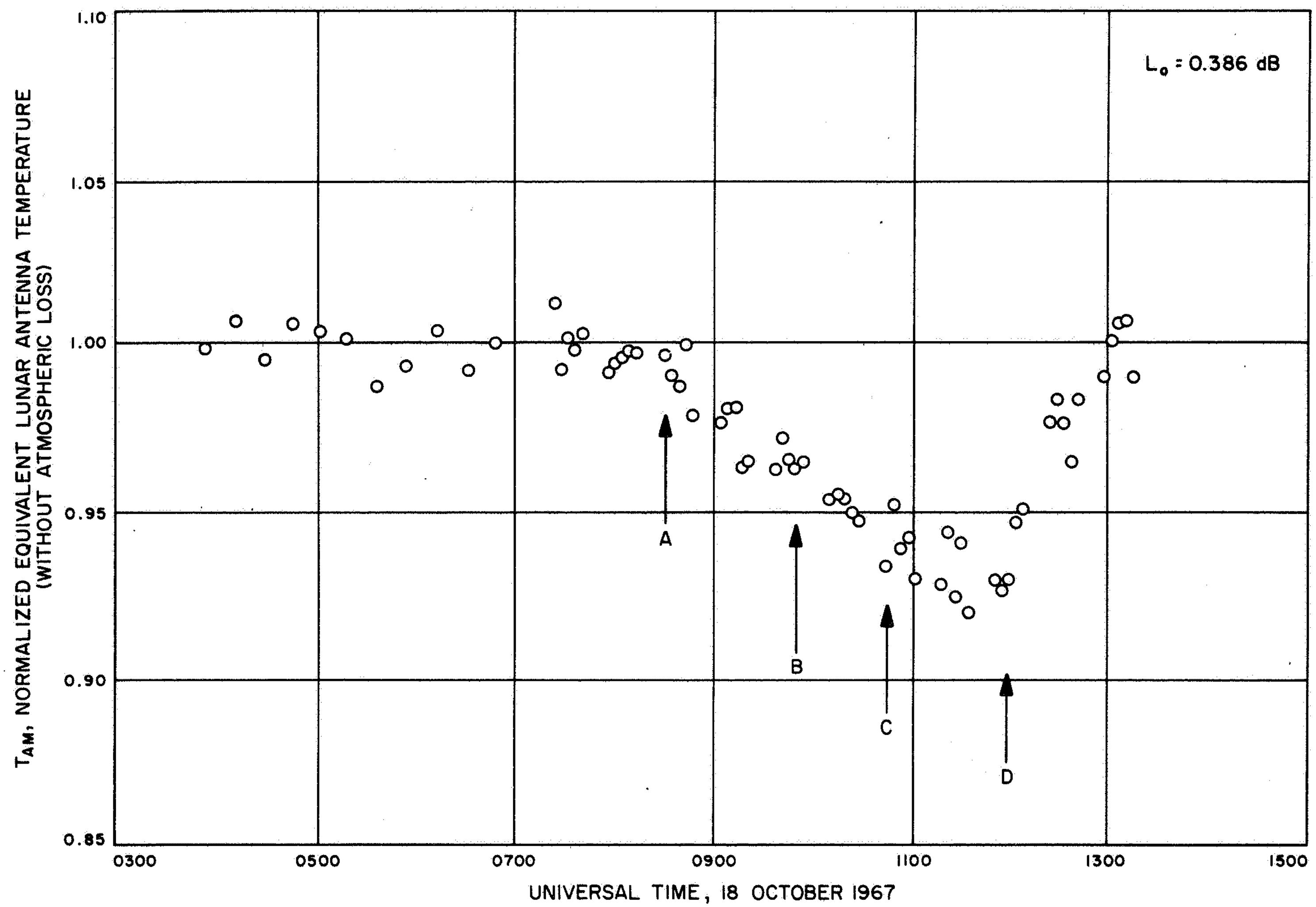


Figure IV-6. Equivalent lunar antenna temperature during night of eclipse, using electronic baseline ($L_O$ = 0.386 dB).

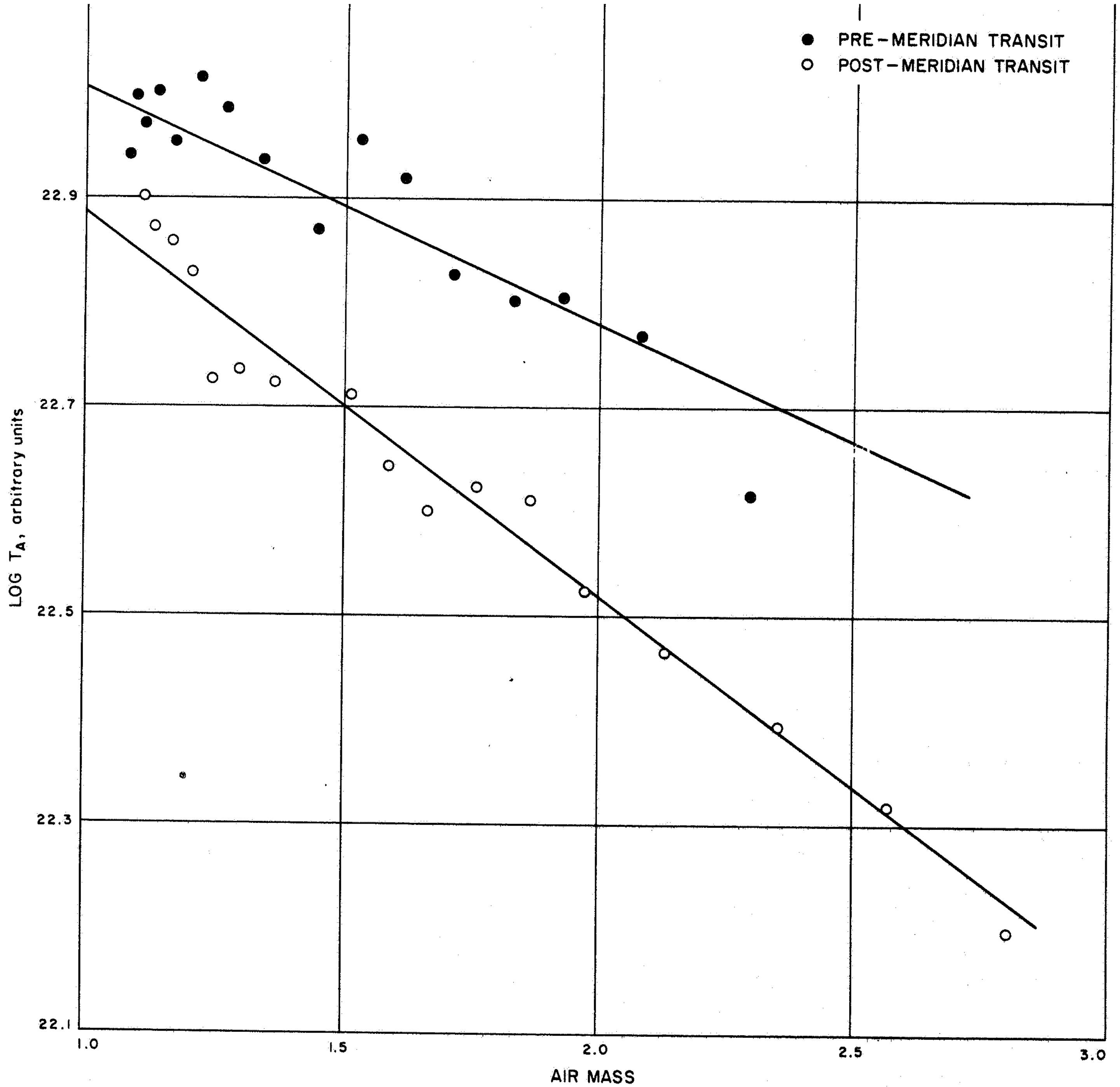


Figure IV-7. Lunar extinction curve during night after eclipse (19 October 1967).

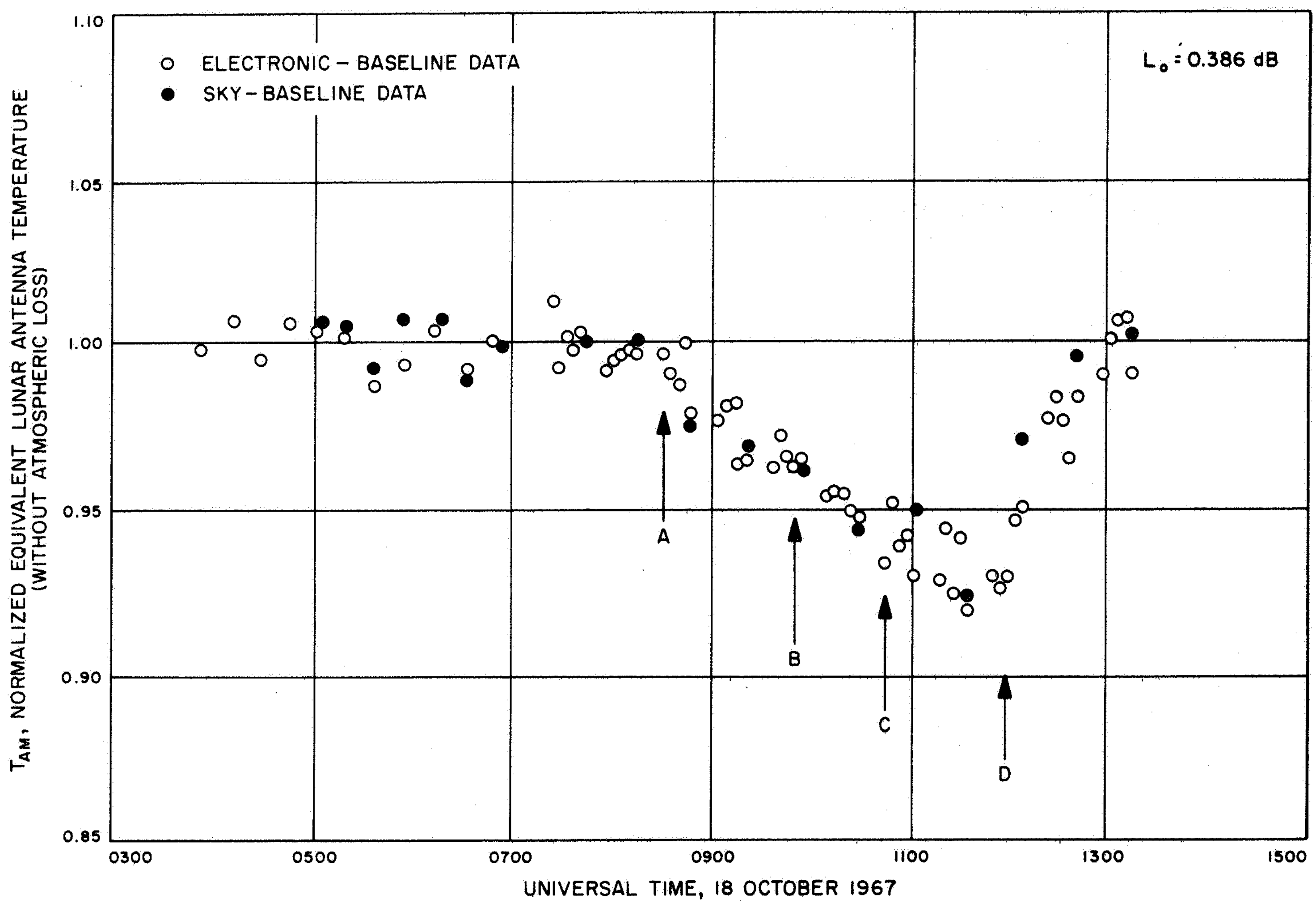


Figure IV-8. Equivalent lunar antenna temperature during night of eclipse, using sky and electronic baselines ($L_o$ = 0.386 dB).

## V. EFFECTS OF VARIABLE ATMOSPHERIC CONDITIONS

One of the most serious problems in the interpretation of radio-astronomical data at millimeter-wavelengths is the effect of changing atmospheric loss. Systematic changes in weather-dependent parameters may introduce significant bias errors which are completely unexplained by normal statistical data fluctuation. Furthermore, these bias errors may be hidden in such a way that considerable effort is involved in their detection. The analysis below is a first attempt to remove one type of systematic change from a set of data points.

The basic equation relating a measured antenna temperature, y, with a source temperature, a, is

$$y = a(e^{-\alpha \ell}) \tag{V-1}$$

where $\alpha$ is the power attenuation constant, nepers/meter. $\ell$, the path length through the homogeneous atmosphere is (for small angles) $\ell_o$ sec Z, where Z is the zenith angle and $\ell_o$ the zenith path length. The atmospheric loss is then given by

$$L = L_o^{\sec Z}$$

where $L_o$ is the atmospheric loss at zenith. If the atmospheric attenuation is assumed to vary linearly with time

$$\alpha = \alpha_0 + \alpha_1 t \tag{V-2}$$

Equation (V-1) becomes

$$y = a(e^{\alpha_0 \ell_0} e^{\alpha_1 \ell_0 t})^{-\sec Z} \tag{V-3}$$

For the analysis that follows, Equation (V-3) has been written symbolically as

$$y = a(be^{ct})^{-\sec Z} \tag{V-4}$$

The quantity $(be^{ct})$ is the zenith loss at any given time; c may be positive or negative; and t is defined as the hours past the first data point. Hence b is the zenith loss at the time of the first data point. (In the analysis to follow the source is assumed to set throughout the period of the observations.) Then, in terms of the declination of the source, $\delta$, and the latitude of the observer, $\Psi$

$$t = \frac{12}{\pi}\left\{\cos^{-1}\left[\frac{\cos Z - \sin\Psi \sin\delta}{\cos\Psi\cos\delta}\right] - \cos^{-1}\left[\frac{\cos Z_1 - \sin\Psi\sin\delta}{\cos\Psi\cos\delta}\right]\right\} \tag{V-5}$$

In order to illustrate the effects of changing atmospheric loss, a set of five data points have been prepared using a = 1.0, b = 1.1, c = 0.1, and assuming that the declination of the source is +26.0 degrees, and the latitude of the observer is +34.2 degrees. The resulting data are presented in Table V-1:

| Data Point Number | Zenith Angle | t | $be^{ct}$ | y |
|---|---|---|---|---|
| 1 | 30.0 | 0.00 | 1.100 | .896 |
| 2 | 40.0 | 0.81 | 1.193 | .795 |
| 3 | 50.0 | 1.62 | 1.293 | .671 |
| 4 | 60.0 | 2.43 | 1.389 | .508 |
| 5 | 70.0 | 3.27 | 1.526 | .291 |

These data are plotted in Figure V-1 using standard extinction curve coordinates. The ordinate is $\log_{10} y$; the abscissa is sec Z. It is clear from Equation (V-4) that the data points will lie on straight lines emanating from the value a = 1.0 on the ordinate axis, the inverse slope of each line being simply $be^{ct}$, the instantaneous loss at that time. However, if the resulting five data points are to be interpreted in terms of a time-independent homogeneous atmosphere, the resulting extinction line through the five points (dashed line) intersects the ordinate axis at 1.81, thus introducing an error of 81% in the value of a. (The equivalent loss would be interpreted as 1.88.)

Realizing that treatment of data received through a time-varying atmosphere must be undertaken using more sophisticated analyses than the standard treatment of time-independent data, a linearized data-fitting procedure was developed to determine the three parameters, a, b, c defined in Equation (V-4). The main points of this analysis are reproduced below:

A set of zero-order solutions $a = a_0$, $b = b_0$, $c = 0$ is determined using the analysis for a time-independent atmosphere.[1] These values then yield $y_0 = a_0(b_0)^{-\sec Z}$. Equation (V-4) is expanded as a truncated Taylor series:

$$y = y_0 + \frac{\partial y}{\partial a}\bigg|_{y_0}(a - a_0) + \frac{\partial y}{\partial b}\bigg|_{y_0}(b-b_0) + \frac{\partial y}{\partial c}\bigg|_{y_0}(c-c_0) \qquad \text{(V-6)}$$

where

---

[1] C. T. Stelzried and W. V. T. Rusch, "Improved Determination of Atmospheric Opacity from Radio Astronomy Measurements", Jour. Geophys. Res., Vol. 72, No. 9, May 1, 1967.

$$\left.\frac{\partial y}{\partial a}\right|_{y_0} = \frac{y_0}{a_0} \tag{V-7}$$

$$\left.\frac{\partial y}{\partial b}\right|_{y_0} = -(\sec Z)\frac{y_0}{b_0} \tag{V-8}$$

$$\left.\frac{\partial y}{\partial b}\right|_{y_0} = -(t \sec Z)y_0 \tag{V-9}$$

Equation (V-6) then becomes

$$y = y_0 + \frac{y_0}{a_0}(a-a_0) - \frac{y_0}{b_0}\sec Z(b-b_0) - y_0(t \sec Z)(c-c_0) \tag{V-10}$$

A measured value $y_m$ corresponds to each pair of the independent variables $Z(t)$ and $t$. Consequently a variance can be defined:

$$\sigma^2 = \Sigma\ (y-y_m)^2 \tag{V-11}$$

where the summation is carried out over all the data points.

Then, the three equations

$$\frac{\partial\sigma^2}{\partial a} = 0; \quad \frac{\partial\sigma^2}{\partial b} = 0; \quad \frac{\partial\sigma^2}{\partial c} = 0 \tag{V-12}$$

are used to generate the following

$$(a-a_0)\left[\frac{\Sigma\, y_0^2}{a_0}\right] + (b-b_0)\left[\frac{\Sigma\, y_0^2 \sec Z}{b_0}\right] + (c-c_0)\left[-\Sigma\, y_0^2 t \sec Z\right] = \Sigma\, y_0(y_m-y_0) \tag{V-13}$$

$$(a-a_0)\left[\frac{\Sigma\, y_0^2 \sec Z}{a_0}\right] + (b-b_0)\left[\frac{-\Sigma\, y_0^2 \sec^2 Z}{b_0}\right] + (c-c_0)\left[-\Sigma\, y_0^2 t \sec^2 Z\right] = \Sigma\, y_0(y_m-y_0)\sec Z \tag{V-14}$$

$$(a-a_0)\left[\frac{\Sigma y_0^2 t \sec Z}{a_0}\right] + (b-b_0)\left[\frac{-\Sigma y_0^2 t \sec^2 Z}{b_0}\right] + (c-c_0)\left[-\Sigma y_0^2 t^2 \sec^2 Z\right] = \Sigma y_0 (y_m - y_0) t \sec Z$$

(V-15)

Inverting these equations yields

$$a = a_0 + \Delta_{0a}/\Delta_0 \qquad \text{(V-16)}$$

$$b = b_0 + \Delta_{0b}/\Delta_0 \qquad \text{(V-17)}$$

$$c = c_0 + \Delta_{0c}/\Delta_0 \qquad \text{(V-18)}$$

where the system determinants $\Delta_{0a}$, $\Delta_{0b}$, $\Delta_{0c}$, and $\Delta_0$ are obtained using Cramer's Rule.

Iteration of Equations (V-16) through (V-18) has generally been found to converge to a set of solutions for a, b, and c. For example, the hypothetical data tabulated in Table V-1 were used in the above set of equations, yielding, after 6 iterations,

$$a = 1.0019 \pm .0011 \text{ p. e.}$$

$$b = 1.1018 \pm .0941 \text{ p. e.}$$

$$c = .0997 \pm .0002 \text{ p. e.}$$

These values compare favorably with the original values of a = 1.0, b = 1.1, and c = 0.1.

The technique outlined above is very sensitive to the number of data points and to random errors in the data points. Attempts to use actual radio-astronomical data have been only marginally successful. However, it is felt that the technique is a useful first step in the determination of time-dependent atmospheric loss, and investigations along similar lines are planned to continue.

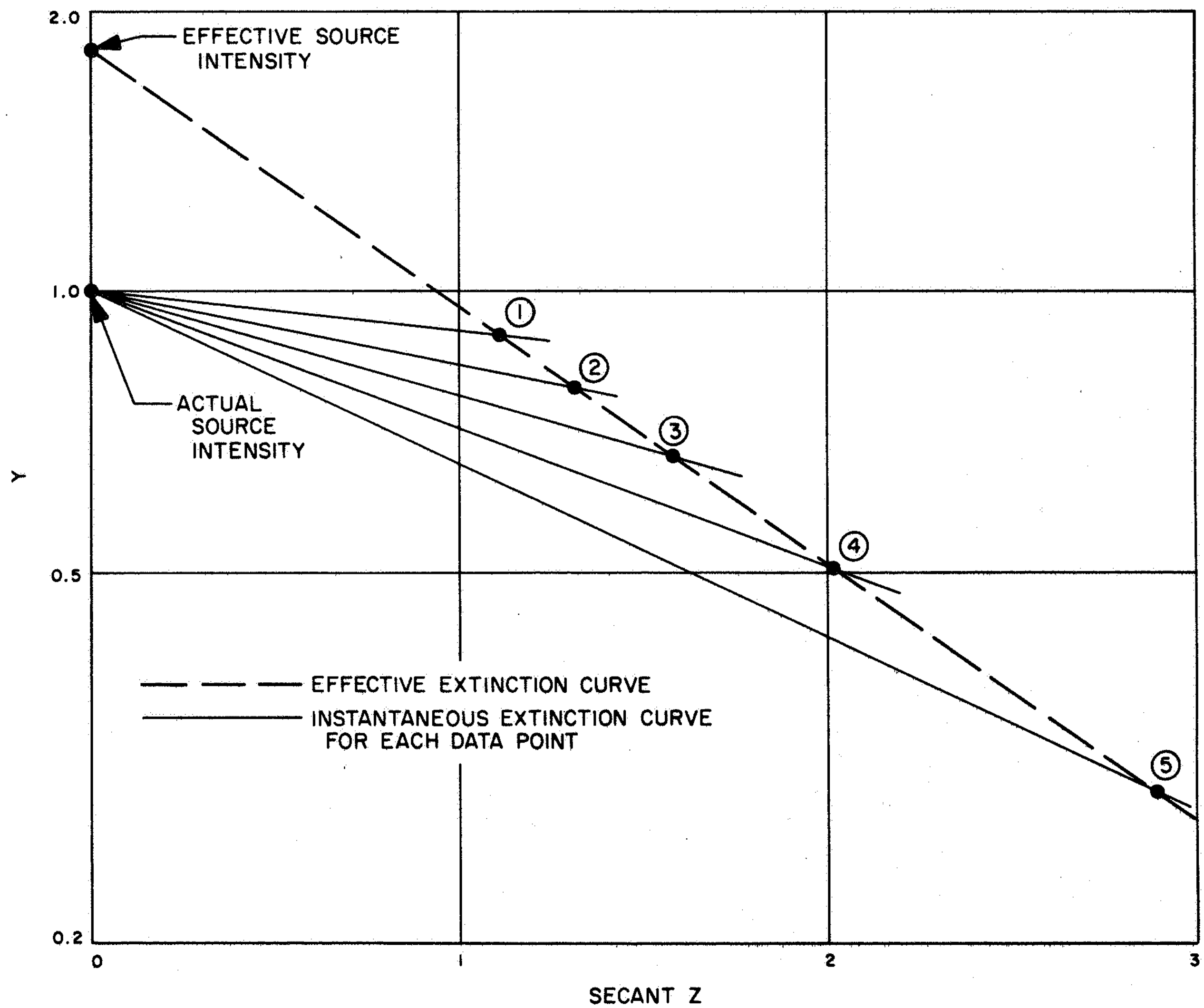


Figure V-1. Determination of incorrect effective source intensity due to changing atmospheric attenuation.

```
      DIMENSION SUM(4),SUMT(4),DATE(18)
      DIMENSION SUM(4),SUMT(4),DATE(18)
      READ (5,1000,END=500) DATE
      READ (5,1001)LOOPA,LOOPB,IPRNT
      READ (5,1002)THES,DELTHE,THENUM
      READ (5,1002)PHIS,DELPHI,PHINUM
      READ (5,1002)THEO,CEP,E,ALPHA,CAYX,CAYZ,CAYOF
      LPRNT=0
      LOOPA=(LOOPA/2)*2
      LOOPB=(LOOPB/2)*2
      PI=3.14159265
      PI2=6.2831853
      PIH=1.5707963
      DEG=.174532925E-01
      RAD=57.2957795
      WRITE (6,4000)DATE
      WRITE (6,5000)
      WRITE (6,5001)THES,DELTHE
      WRITE (6,5002)PHIS,DELPHI
      WRITE (6,5003)THEO,CEP,E,ALPHA
      WRITE (6,5004)CAYX,CAYZ,CAYOF
      ALPHA=ALPHA*DEG
      THES=THES*DEG
      DELTHE=DELTHE*DEG
      PHIS=PHIS*DEG
      THEO=THEO*DEG
      DELPHI=DELPHI*DEG
      DELTH3=(PI-THEO)/FLOAT(LOOPA)
      TEMP=DELTH3*RAD
      WRITE (6,5005)DELTH3,TEMP
      SINA=SIN(ALPHA)
      COSA=COS(ALPHA)
      R1=DELTH3/3.0
      JFK=THENUM
      LBJ=PHINUM
      A=LOOPA
      B=LOOPB
      DEL=(B-4.0)/A
      LOOPA=LOOPA+1
      DO 900 L=1,LBJ
      PHI=PHIS+DELPHI*FLOAT(L-1)
      TEMP=PHI*RAD
      WRITE (6,6000)PHI,TEMP
      WRITE (6,6001)
      WRITE (6,6002)
      SINP=SIN(PHI)
      COSP=COS(PHI)
      DO 800 K=1,JFK
      THE=THES+DELTHE*FLOAT(K-1)
      SINT=SIN(THE)
      COST=COS(THE)
      CTCP=COST*COSP
      DO 30 I=1,4
   30 SUMT(I)=0.0
      CTSP=COST*SINP
      IF(IPRNT)34,35,34
   34 LRUN=1
      WRITE (6,7000)LRUN,SINA,SINP,SINT,CTSP,COSA,COSP, COST,CTCP,THE,DE
```

```
     1L
  35 LL=1
     DO 600 J=1,LOOPA
     FLOT=J-1
     THE3=THE0+DELTH3*FLOT
     NN=B+0.5-DEL*FLOT
     NN=(NN/2)*2
     DELPH3=PI2/FLOAT(NN)
     R2=DELPH3/3.0
     NN=NN+1
     SINT3=SIN(THE3)
     COST3=COS(THE3)
     T1=1.0+E*COST3
     CAYRO3=-CEP/T1
     CAYZ3=CAYRO3*COST3
     ECOST3=E+COST3
     SAECT3=SINA*ECOST3
     FTHETA=SINT3/(T1*T1)
     R3=FTHETA*R2
     R4=R3*2.0
     R5=R3*4.0
     DO 40 I=1,4
  40 SUM(I)=0.0
     IF(IPRNT)41,42,41
  41 LRUN=2
     TEMP=DELPH3*RAD
     WRITE (6,7001)LRUN,THE3,T1,CAYRO3,R3,SINT3,ECOST3, CAYZ3,R4,COST3,
    1SAECT3,FTHETA,R5,DELPH3,TEMP
  42 KK=1
     DO 400 I=1,NN
     PHI3=DELPH3*FLOAT(I-1)
     SINP3=SIN(PHI3)
     COSP3=COS(PHI3)
     ST3CP3=SINT3*COSP3
     ST3SP3=SINT3*SINP3
     CAYX3=CAYRO3*ST3CP3
     CAYY3=CAYRO3*ST3SP3
     CAYX1=CAYX3*COSA-CAYZ3*SINA-CAYX
     CAYY1=CAYY3
     CAYZ1=CAYX3*SINA+CAYZ3*COSA-CAYZ
     T2=CAYX1**2+CAYY1**2
     CAYRO1=SQRT(T2+CAYZ1**2)
     T3=SQRT(T2)
     THE1=PI-ATAN(T3/ABS(CAYZ1))
     PHI1=ARCOS(ABS(CAYX1)/T3)
     IF(CAYX1)70,50,50
  50 IF(CAYY1)60,100,100
  60 PHI1=PI2-PHI1
     GO TO 100
  70 IF(CAYY1)80,90,90
  80 PHI1=PI+PHI1
     GO TO 100
  90 PHI1=PI-PHI1
 100 CAYX2=CAYX1
     CAYY2=CAYY1
     CAYZ2=CAYZ1+CAYOF
     CAYRO2=SQRT(T2+CAYZ2**2)
     IF(CAYZ2)110,130,120
```

```
.10 THE2=PI-ATAN(T3/ABS(CAYZ2))
    GO TO 140
.20 THE2=ATAN(T3/CAYZ2)
    GO TO 140
.30 THE2=PIH
.40 PHI2=PHI1
    CC=COSA*ST3CP3-SINA*ECOST3
    DD=ST3SP3
    EE=SINA*ST3CP3+COSA*ECOST3
    SINT1=SIN(THE1)
    COST1=COS(THE1)
    SINP1=SIN(PHI1)
    COSP1=COS(PHI1)
    FF=(1.0+COST1)*SINP1*COSP1
    GG=COST1*SINP1*SINP1-COSP1*COSP1
    HH=-SINT1*SINP1
    T4=DD*HH-EE*GG
    T5=EE*FF-CC*HH
    T6=CC*GG-DD*FF
    AM=T4*CTCP+T5*CTSP-T6*SINT
    AN=T5*COSP-T4*SINP
    LMAG=0
    CALL OPTION(THE1,ANS,L,LMAG)
    AA=ANS
    LMAG=1
    CALL OPTION(THE1,ANS,L,LMAG)
    BB=ANS
    T7=CAYRO3/CAYRO1
    G1=T7*AM
    G2=T7*AN
    T8=COS(PHI-PHI2)
    T9=SINT*SIN(THE2)
    S1=COST*COS(THE2)
    H=CAYRO2*(T9*T8+S1)-CAYRO1
    SINH=SIN(H)
    COSH=COS(H)
    S2=AA*COSH-BB*SINH
    S3=BB*COSH+AA*SINH
    IF(I-LOOPB)170,200,170
170 GO TO(200,220,240),KK
200 SUM(1)=SUM(1)+G1*S2
    SUM(2)=SUM(2)+G1*S3
    SUM(3)=SUM(3)+G2*S2
    SUM(4)=SUM(4)+G2*S3
    KK=3
    GO TO 300
220 SUM(1)=SUM(1)+G1*S2*2.0
    SUM(2)=SUM(2)+G1*S3*2.0
    SUM(3)=SUM(3)+G2*S2*2.0
    SUM(4)=SUM(4)+G2*S3*2.0
    KK=3
    GO TO 300
240 SUM(1)=SUM(1)+G1*S2*4.0
    SUM(2)=SUM(2)+G1*S3*4.0
    SUM(3)=SUM(3)+G2*S2*4.0
    SUM(4)=SUM(4)+G2*S3*4.0
    KK=2
300 IF(IPRNT)305,400,305
```

```
305 LRUN=3
    WRITE (6,7002)LRUN,PHI3,THE1,SINT1,CAYX1,SINP3,THE2, COST1,CAYY1,C
   1OSP3,PHI1,SINP1,CAYZ1
    WRITE (6,7003)ST3CP3,PHI2,COSP1,T2,ST3SP3,CAYX3, CAYY3,T3,T4,T5,T6
   1,T7
    WRITE (6,7004)T8,T9,S1,S2,S3,CAYX2,CAYRO1,AA,H, CAYY2,G1,BB
    WRITE (6,7005)SINH,CAYZ2,G2,CC,COSH,AM,AN, DD,EE,FF,GG,HH,CAYRO2
    WRITE (6,7006)SUM(1),SUM(2),SUM(3),SUM(4), SUMT(1),SUMT(2),SUMT(3)
   1,SUMT(4)
    LPRNT=LPRNT+1
    IF(LPRNT-IPRNT)400,400,310
310 IPRNT=0
400 CONTINUE
    IF(J-LOOPA)420,440,420
420 GO TO(440,460,480),LL
440 SUMT(1)=SUMT(1)+SUM(1)*R3
    SUMT(2)=SUMT(2)+SUM(2)*R3
    SUMT(3)=SUMT(3)+SUM(3)*R3
    SUMT(4)=SUMT(4)+SUM(4)*R3
    LL=3
    GO TO 600
460 SUMT(1)=SUMT(1)+SUM(1)*R4
    SUMT(2)=SUMT(2)+SUM(2)*R4
    SUMT(3)=SUMT(3)+SUM(3)*R4
    SUMT(4)=SUMT(4)+SUM(4)*R4
    LL=3
    GO TO 600
480 SUMT(1)=SUMT(1)+SUM(1)*R5
    SUMT(2)=SUMT(2)+SUM(2)*R5
    SUMT(3)=SUMT(3)+SUM(3)*R5
    SUMT(4)=SUMT(4)+SUM(4)*R5
    LL=2
600 CONTINUE
    DO 650 I=1,4
650 SUMT(I)=SUMT(I)*R1
    TEMP=THE*RAD
    CALL PHASE(SUMT(1),SUMT(2),TEMS)
    CALL PHASE(SUMT(3),SUMT(4),TEMT)
    T1=SQRT(SUMT(1)**2+SUMT(2)**2)
    T2=SQRT(SUMT(3)**2+SUMT(4)**2)
    WRITE (6,6003)TEMP,SUMT(1),SUMT(2),T1,TEMS, SUMT(3),SUMT(4),T2,TEM
   1T
800 CONTINUE
900 CONTINUE
    GO TO 1
.000 FORMAT(18A4)
.001 FORMAT(14I5)
.002 FORMAT(7F10.0)
.000 FORMAT(1H1,30X,18A4)
i000 FORMAT(39H0INPUT PARAMETERS AND CONTROL CONSTANTS)
i001 FORMAT(7H0THETA=F12.5,8H DEGREES,10X,10HINCREMENT=F12.5)
i002 FORMAT(5H PHI=F12.5,8H DEGREES,12X,10HINCREMENT=F12.5)
i003 FORMAT(10H0THETA(0)=F12.5,10X,3HKEP,6X,1H=,F12.5,10X,1HE,8X,1H=,
   1F12.5,10X,10HALPHA     =F12.5)
i004 FORMAT(3H KX,6X,1H=F12.5,10X,2HKZ,7X,1H=F12.5,10X,3HKOF,6X,
   11H=F12.5)
i005 FORMAT(21H0OUTER INTEGRAL STEP=F12.5,10H RADIANS =F12.5,8H DEGREES
   1)
```

```
)00 FORMAT(5H1PHI=F12.5,9H RADIANS=F12.5,8H DEGREES)
)01 FORMAT(7H0 THETA,28X,7HE THETA,50X,5HE PHI)
J02 FORMAT(8H0DEGREES,2(8X,4HREAL,8X,9HIMAGINARY,6X,9HMAGNITUDE,
   16X,6HPHASE ))
)03 FORMAT(F8.3,2(3F15.8,F11.3))
)00 FORMAT(1H0,I2,4X,7HSINA   =F15.8,8X,7HSINP   =F15.8,8X,7HSINT   =F15.
   18,8X,7HCTSP   =F15.8/7X,7HCOSA   =F15.8,8X,7HCOSP   =F15.8,8X,7HCOST
   2 =F15.8,8X,7HCTCP   =F15.8/7X,7HTHE    =F15.8,8X,7HDEL    =F15.8)
)01 FORMAT(1H0,I2,4X,7HTHE3   =F15.8,8X,7HT1     =F15.8,8X,7HCAYR03=F15.
   18,8X,7HR3     =F15.8/7X,7HSINT3 =F15.8,8X,7HECOST3=F15.8,8X,7HCAYZ3
   2 =F15.8,8X,7HR4     =F15.8/7X,7HCOST3 =F15.8,8X,7HSAECT3=F15.8,8X,
   37HFTHETA=F15.8,8X,7HR5     =F15.8/7X,7HDELPH3=F15.8,8X,7HIN DEG=F15
   4.8)
002 FORMAT(1H0,I2,4X,7HPHI3   =F15.8,8X,7HTHE1   =F15.8,8X,7HSINT1 =F15.
   18,8X,7HCAYX1 =F15.8/7X,7HSINP3 =F15.8,8X,7HTHE2   =F15.8,8X,7HCOST1
   2 =F15.8,8X,7HCAYY1 =F15.8/7X,7HCOSP3 =F15.8,8X,7HPHI1   =F15.8,8X,
   37HSINP1 =F15.8,8X,7HCAYZ1 =F15.8)
003 FORMAT(7X,7HST3CP3=F15.8,8X,7HPHI2   =F15.8,8X,7HCOSP1 =F15.8,8X,7H
   1T2     =F15.8/7X,7HST3SP3=F15.8,8X,7HCAYX3 =F15.8,8X,7HCAYY3 =F15.8
   2,8X,7HT3     =F15.8/7X,7HT4     =F15.8,8X,7HT5     =F15.8,8X,7HT6
   3=F15.8,8X,7HT7     =F15.8)
004 FORMAT(7X,7HT8     =F15.8,8X,7HT9     =F15.8,8X,7HS1     =F15.8,8X,7H
   1S2     =F15.8/7X,7HS3     =F15.8,8X,7HCAYX2 =F15.8,8X,7HCAYR01=F15.8
   2,8X,7HAA     =F15.8/7X,7HH      =F15.8,8X,7HCAYY2 =F15.8,8X,7HG1
   3=F15.8,8X,7HBB     =F15.8)
005 FORMAT(7X,7HSINH   =F15.8,8X,7HCAYZ2 =F15.8,8X,7HG2     =F15.8,8X,7H
   1CC     =F15.8/7X,7HCOSH   =F15.8,8X,7HAM     =F15.8,8X,7HAN     =F15.8
   2,8X,7HDD     =F15.8/7X,7HEE     =F15.8,8X,7HFF     =F15.8,8X,7HGG
   3=F15.8,8X,7HHH     =F15.8/7X,7HCAYR02=F15.8)
006 FORMAT(7X,7HSUM  1=F15.8,8X,7HSUM  2=F15.8,8X,7HSUM  3=F15.8,8X,7H
   1SUM  4=F15.8/7X,7HSUMT 1=F15.8,8X,7HSUMT 2=F15.8,8X,7HSUMT 3=F15.8
   2,8X,7HSUMT 4=F15.8)
0    STOP
     END
```

```
      SUBROUTINE PHASE(A,B,C)                                           PHAS0020
      C=0.0                                                             PHAS0030
      IF(A)20,5,20                                                      PHAS0040
    5 IF(B)75,100,100                                                   PHAS0050
   20 TEMP=B/A                                                          PHAS0060
      C=ATAN(ABS(TEMP))*57.2957795                                      PHAS0070
      IF(TEMP)30,60,70                                                  PHAS0080
   30 IF(B)50,50,40                                                     PHAS0090
   40 C=180.0-C                                                         PHAS0100
      GO TO 100                                                         PHAS0110
   50 C=360.0-C                                                         PHAS0120
      GO TO 100                                                         PHAS0130
   60 IF(A)75,100,100                                                   PHAS0140
   70 IF(B)75,75,100                                                    PHAS0150
   75 C=180.0+C                                                         PHAS0160
  100 RETURN                                                            PHAS0170
      END                                                               PHAS0180
```

```
      SUBROUTINE OPTION(THE1,ANS,L,LMAG)
      ANS=0.0
      IF(LMAG)5,5,30
    5 X=SIN(THE1)
      Y=13.375*X
      Z=SIN(Y)*COS(Y)
      V=(1.0-72.48*X*X)*Y
      ANS=Z/V
   30 RETURN
      END
```

OCTOBER 1967 DATA FROM TOTAL LUNAR ECLIPSE OBSERVATIONS

| DAY NUM | LOCAL* TIME** | ELEVA TION* | MOON*SWITCH* AVERAGE | **PE* | HOTLOADSWTCH AVERAGE | **PE* | BASENOSWITCH AVERAGE | **PE* | BASE**SWITCH AVERAGE | **PE* | TEMP** DEG*C* |
|---|---|---|---|---|---|---|---|---|---|---|---|
| 290 | 190736 | 13.12 | 5.5123 | .0438 | 4.2656 | .0328 | 1.4881 | .0015 | 1.4199 | .0210 | |
| 290 | 192648 | 16.97 | 5.6504 | .0362 | 4.1181 | .0376 | 1.4806 | .0037 | 1.4026 | .0272 | |
| 290 | 194612 | 20.86 | 5.7909 | .0304 | 4.1032 | .0262 | 1.4582 | .0012 | 1.4116 | .0252 | 111.08 |
| 290 | 200400 | 24.42 | 5.9082 | .0362 | 4.1780 | .0307 | 1.4860 | .0019 | 1.4753 | .0735 | 110.96 |
| 290 | 202024 | 27.68 | 6.0353 | .0581 | 4.1054 | .0496 | 1.4770 | .0026 | 1.4379 | .0657 | 110.87 |
| 290 | 205224 | 33.96 | 5.5821 | .0276 | 4.0250 | .0233 | 1.5096 | .0015 | 1.4058 | .0114 | 113.58 |
| 290 | 211212 | 37.77 | 5.6643 | .0215 | 3.9696 | .0138 | 1.5125 | .0013 | 1.4144 | .0062 | 111.92 |
| 290 | 212900 | 40.93 | 5.6642 | .0151 | 3.9865 | .0220 | 1.5306 | .0018 | 1.5025 | .0215 | 111.11 |
| 290 | 214612 | 44.09 | 5.7470 | .0160 | 3.9461 | .0112 | 1.5432 | .0007 | 1.4253 | .0218 | 110.74 |
| 290 | 220300 | 47.07 | 5.7608 | .0083 | 3.9252 | .0217 | 1.5482 | .0007 | 1.4922 | .0205 | 110.55 |
| 290 | 221848 | 49.66 | 5.7658 | .0134 | 3.9282 | .0203 | 1.5506 | .0010 | 1.4894 | .0061 | 110.47 |
| 290 | 223700 | 52.68 | 5.6968 | .0225 | 3.8925 | .0096 | 1.5314 | .0022 | 1.4598 | .0122 | 110.43 |
| 290 | 225412 | 55.23 | 5.7379 | .0115 | 3.9356 | .0154 | 1.5384 | .0016 | 1.4302 | .0162 | 110.45 |
| 290 | 231324 | 57.76 | 5.7725 | .0201 | 3.8995 | .0152 | 1.5252 | .0012 | 1.4678 | .0151 | 110.50 |
| 290 | 233212 | 59.84 | 5.7180 | .0094 | 3.9191 | .0235 | 1.5228 | .0010 | 1.4870 | .0234 | 110.53 |
| 290 | 234836 | 61.27 | 5.7452 | .0160 | 3.9076 | .0069 | 1.5166 | .0009 | 1.4675 | .0179 | 110.48 |
| 291 | 002424 | 62.85 | 5.8084 | .0223 | | | 1.5406 | .0011 | | | |
| 291 | 002824 | 62.88 | 5.7026 | .0239 | | | 1.5206 | .0023 | | | |
| 291 | 003236 | 62.88 | 5.7537 | .0092 | | | 1.5330 | .0011 | | | |
| 291 | 003648 | 62.85 | 5.7398 | .0154 | | | 1.5376 | .0014 | | | |
| 291 | 004100 | 62.78 | 5.7363 | .0095 | 3.9418 | .0102 | 1.5152 | .0007 | 1.4615 | .0127 | 110.45 |
| 291 | 005700 | 62.24 | 5.6776 | .0147 | | | 1.5158 | .0020 | | | |
| 291 | 010100 | 62.03 | 5.6717 | .0111 | | | 1.5010 | .0014 | | | |
| 291 | 010512 | 61.78 | 5.6794 | .0161 | | | 1.5050 | .0017 | | | |
| 291 | 010936 | 61.49 | 5.6866 | .0069 | | | 1.5086 | .0011 | | | |
| 291 | 011348 | 61.19 | 5.7045 | .0107 | 3.9366 | .0148 | 1.5310 | .0028 | 1.4781 | .0157 | 110.36 |
| 291 | 013012 | 59.74 | 5.6861 | .0231 | | | 1.5290 | .0011 | | | |
| 291 | 013424 | 59.30 | 5.6635 | .0094 | | | 1.5358 | .0013 | | | |
| 291 | 013900 | 58.81 | 5.6452 | .0208 | | | 1.5360 | .0006 | | | |
| 291 | 014300 | 58.35 | 5.6831 | .0179 | | | 1.5254 | .0012 | | | |
| 291 | 014700 | 57.88 | 5.5962 | .0125 | 3.8110 | .0121 | 1.5328 | .0017 | 1.4940 | .0320 | 110.30 |
| 291 | 020424 | 55.62 | 5.5665 | .0111 | | | 1.5318 | .0027 | | | |
| 291 | 020836 | 55.04 | 5.5782 | .0165 | | | 1.5290 | .0013 | | | |
| 291 | 021248 | 54.43 | 5.5722 | .0181 | | | 1.5268 | .0009 | | | |
| 291 | 021700 | 53.82 | 5.4957 | .0186 | | | 1.5308 | .0015 | | | |
| 291 | 022112 | 53.19 | 5.5037 | .0097 | 3.9107 | .0150 | 1.5382 | .0018 | 1.4820 | .0172 | 110.58 |
| 291 | 023712 | 50.68 | 5.4652 | .0271 | | | 1.5314 | .0013 | | | |
| 291 | 024124 | 49.99 | 5.4998 | .0148 | | | 1.5350 | .0006 | | | |
| 291 | 024536 | 49.30 | 5.4650 | .0261 | | | 1.5312 | .0011 | | | |
| 291 | 024948 | 48.59 | 5.4464 | .0228 | | | 1.5306 | .0022 | | | |
| 291 | 025412 | 47.85 | 5.4441 | .0109 | 3.9161 | .0087 | 1.5278 | .0013 | 1.4821 | .0120 | 110.90 |
| 291 | 031112 | 44.88 | 5.3763 | .0176 | | | 1.5356 | .0009 | | | |
| 291 | 031524 | 44.14 | 5.3699 | .0125 | | | 1.5344 | .0021 | | | |
| 291 | 031948 | 43.34 | 5.3448 | .0202 | | | 1.5212 | .0027 | | | |
| 291 | 032400 | 42.58 | 5.3292 | .0183 | | | 1.5328 | .0015 | | | |
| 291 | 032824 | 41.78 | 5.3010 | .0095 | 3.8714 | .0162 | 1.5246 | .0009 | 1.4941 | .0124 | 111.11 |

| | | | | | | | | | | | | |
|---|---|---|---|---|---|---|---|---|---|---|---|---|
| D | 291 | 034512 | 38.67 | 5.2269 | .0122 | | | 1.5448 | .0021 | | | |
| D | 291 | 034936 | 37.84 | 5.2949 | .0177 | | | 1.5514 | .0011 | | | |
| D | 291 | 035348 | 37.05 | 5.2376 | .0237 | | | 1.5568 | .0030 | | | |
| D | 291 | 035800 | 36.25 | 5.2404 | .0127 | | | 1.5600 | .0010 | | | |
| D | 291 | 040224 | 35.42 | 5.1953 | .0115 | 3.9179 | .0152 | 1.5758 | .0009 | 1.4561 | .0095 | 111.34 |
| D | 291 | 041800 | 32.43 | 5.1204 | .0153 | | | 1.5586 | .0013 | | | |
| D | 291 | 042200 | 31.65 | 5.1546 | .0116 | | | 1.5452 | .0012 | | | |
| D | 291 | 042624 | 30.80 | 5.0748 | .0102 | | | 1.5578 | .0011 | | | |
| D | 291 | 043048 | 29.95 | 5.1140 | .0121 | | | 1.5504 | .0010 | | | |
| D | 291 | 043500 | 29.13 | 5.0125 | .0193 | 3.8584 | .0148 | 1.5474 | .0003 | 1.4952 | .0113 | 111.68 |
| D | 291 | 045048 | 26.04 | 4.9746 | .0144 | | | 1.5466 | .0010 | | | |
| D | 291 | 045500 | 25.22 | 4.9365 | .0157 | | | 1.5424 | .0022 | | | |
| D | 291 | 045912 | 24.40 | 4.9291 | .0291 | | | 1.5458 | .0047 | | | |
| D | 291 | 050336 | 23.53 | 4.9656 | .0201 | | | 1.5458 | .0023 | | | |
| D | 291 | 050748 | 22.71 | 4.9547 | .0148 | 3.8928 | .0242 | 1.5472 | .0051 | 1.4337 | .0154 | 111.48 |
| D | 291 | 052412 | 19.48 | 4.9060 | .0160 | | | 1.5324 | .0011 | | | |
| D | 291 | 052824 | 18.65 | 4.8849 | .0128 | | | 1.5274 | .0017 | | | |
| D | 291 | 053236 | 17.82 | 4.8481 | .0100 | | | 1.5570 | .0016 | | | |
| D | 291 | 053700 | 16.96 | 4.7594 | .0064 | | | 1.5540 | .0003 | | | |
| D | 291 | 054100 | 16.17 | 4.7779 | .0066 | 3.8574 | .0114 | 1.5554 | .0016 | 1.4719 | .0157 | 111.60 |
| D | 291 | 055712 | 12.99 | 4.5919 | .0151 | | | 1.5786 | .0011 | | | |
| D | 291 | 060124 | 12.17 | 4.5415 | .0125 | | | 1.5696 | .0011 | | | |
| D | 291 | 060612 | 11.23 | 4.4528 | .0195 | | | 1.5604 | .0008 | | | |
| D | 291 | 061024 | 10.41 | 4.3466 | .0078 | | | 1.5466 | .0010 | | | |
| D | 291 | 061436 | 09.59 | 4.2241 | .0144 | 3.8093 | .0154 | 1.5734 | .0011 | 1.5072 | .0131 | 111.89 |

NUM = RUN NUMBER
NUM = LOCAL DAY NUMBER
AL TIME = PACIFIC DAYLIGHT TIME
VATION = ELEVATION OF MOON AT LOCAL TIME
N*SWITCH = DIGITAL OUTPUT FOR MOON IN PRIMARY BEAM
LOADSWTCH = DIGITAL OUTPUT FOR HOT LOAD CALIBRATION
ENOSWITCH = DIGITAL OUTPUT FOR ELECTRONIC BASELINE
E**SWITCH = DIGITAL OUTPUT FOR SKY-SKY BASELINE
P** = TEMPERATURE DIFFERENCE BETWEEN HOT AND AMBIENT LOADS
RAGE = AVERAGE DIGITAL OUTPUT
= PROBABLE ERROR OF DIGITAL OUTPUT

APPENDIX C

CTOBER 1967 DATA FROM LUNAR OBSERVATIONS

| DAY | LOCAL* | ELEVA | MOON*SWITCH* | | HOTLOADSWTCH | | BASENOSWITCH | | BASE**SWITCH | | TEMP** |
|---|---|---|---|---|---|---|---|---|---|---|---|
| NUM | TIME** | TION* | AVERAGE** | PE* | AVERAGE** | PE* | AVERAGE** | PE* | AVERAGE** | PE* | DEG*C* |
| 291 | 203600 | 25.82 | 5.1102 | .0131 | 3.6173 | .0118 | 1.3486 | .0009 | 1.3276 | .0166 | 110.30 |
| 291 | 205024 | 28.72 | 5.2198 | .0175 | 3.5956 | .0120 | 1.3198 | .0003 | 1.3738 | .0136 | 109.85 |
| 291 | 210312 | 31.29 | 5.2814 | .0142 | 3.5815 | .0147 | 1.3454 | .0022 | 1.2841 | .0230 | 109.69 |
| 291 | 211212 | 33.09 | 5.2609 | .0154 | 3.5943 | .0077 | 1.3264 | .0010 | 1.3149 | .0096 | 109.54 |
| 291 | 212524 | 35.73 | 5.2906 | .0117 | 3.5435 | .0154 | 1.3304 | .0010 | 1.3005 | .0248 | 109.45 |
| 291 | 213800 | 38.23 | 5.4041 | .0226 | 3.5851 | .0136 | 1.3560 | .0016 | 1.3696 | .0125 | 109.44 |
| 291 | 215100 | 40.78 | 5.4388 | .0172 | 3.6182 | .0131 | 1.3538 | .0021 | 1.3896 | .0096 | 109.44 |
| 291 | 220548 | 43.67 | 5.3687 | .0136 | 3.6226 | .0101 | 1.3612 | .0008 | 1.2690 | .0158 | 109.42 |
| 291 | 223000 | 48.29 | 5.4276 | .0091 | 3.6873 | .0142 | 1.3524 | .0013 | 1.3525 | .0159 | 109.40 |
| 291 | 225000 | 51.98 | 5.4717 | .0198 | 3.6952 | .0161 | 1.3466 | .0015 | 1.3675 | .0167 | 109.36 |
| 291 | 230800 | 55.17 | 5.5092 | .0241 | 3.6690 | .0308 | 1.3526 | .0009 | 1.3634 | .0106 | 109.35 |
| 291 | 232912 | 58.71 | 5.4889 | .0121 | 3.6155 | .0200 | 1.3856 | .0023 | 1.3862 | .0136 | 109.32 |
| 291 | 234800 | 61.56 | 5.5518 | .0113 | 3.6720 | .0094 | 1.3994 | .0029 | 1.3821 | .0142 | 109.28 |
| 292 | 000648 | 64.06 | 5.5446 | .0164 | 3.7272 | .0207 | 1.4184 | .0028 | 1.3549 | .0173 | 109.25 |
| 292 | 002400 | 65.94 | 5.5918 | .0180 | 3.6759 | .0130 | 1.4358 | .0011 | 1.4301 | .0125 | 109.20 |
| 292 | 004236 | 67.42 | 5.5561 | .0111 | 3.7153 | .0051 | 1.4500 | .0004 | 1.3537 | .0160 | 109.23 |
| 292 | 021100 | 64.52 | 5.5661 | .0133 | 3.7916 | .0150 | 1.4754 | .0005 | 1.4506 | .0179 | 109.95 |
| 292 | 023136 | 61.92 | 5.5392 | .0178 | 3.7541 | .0159 | 1.4732 | .0024 | 1.4240 | .0189 | 109.90 |
| 292 | 025048 | 59.02 | 5.5404 | .0205 | 3.7226 | .0075 | 1.4824 | .0010 | 1.4142 | .0119 | 109.88 |
| 292 | 030900 | 56.01 | 5.4796 | .0168 | 3.7761 | .0173 | 1.4460 | .0004 | 1.4344 | .0116 | 109.96 |
| 292 | 032400 | 53.41 | 5.4164 | .0219 | 3.7754 | .0119 | 1.4736 | .0009 | 1.4345 | .0074 | 110.10 |
| 292 | 034024 | 50.46 | 5.4255 | .0072 | 3.7720 | .0163 | 1.4714 | .0017 | 1.4056 | .0125 | 110.23 |
| 292 | 035848 | 47.05 | 5.4201 | .0118 | 3.8377 | .0108 | 1.4732 | .0009 | 1.3899 | .0116 | 110.56 |
| 292 | 042900 | 41.28 | 5.4543 | .0221 | 3.8176 | .0112 | 1.5116 | .0014 | 1.4419 | .0127 | 110.00 |
| 292 | 044048 | 38.99 | 5.3832 | .0114 | 3.9137 | .0127 | 1.5002 | .0009 | 1.4377 | .0140 | 110.98 |
| 292 | 045148 | 36.84 | 5.3654 | .0121 | 3.9216 | .0124 | 1.5186 | .0013 | 1.4448 | .0138 | 110.91 |
| 292 | 050336 | 34.53 | 5.3801 | .0168 | 3.9119 | .0184 | 1.5102 | .0005 | 1.4786 | .0155 | 110.89 |
| 292 | 051436 | 32.36 | 5.3652 | .0138 | 3.8344 | .0161 | 1.5052 | .0012 | 1.4772 | .0127 | 110.88 |
| 292 | 052424 | 30.42 | 5.2806 | .0141 | 3.8419 | .0130 | 1.4944 | .0015 | 1.4305 | .0173 | 110.83 |
| 292 | 053648 | 27.97 | 5.2349 | .0155 | 3.8178 | .0097 | 1.4976 | .0007 | 1.4421 | .0092 | 110.71 |
| 292 | 055112 | 25.13 | 5.1695 | .0168 | 3.8755 | .0194 | 1.4910 | .0014 | 1.4082 | .0103 | 110.52 |
| 292 | 060236 | 22.88 | 5.0880 | .0147 | 3.7394 | .0151 | 1.4708 | .0022 | 1.4137 | .0135 | 110.42 |
| 292 | 061248 | 20.87 | 4.9924 | .0122 | 3.7885 | .0151 | 1.4720 | .0010 | 1.4374 | .0072 | 110.27 |

NUM = RUN NUMBER
NUM = LOCAL DAY NUMBER
L TIME = PACIFIC DAYLIGHT TIME
'ATION = ELEVATION OF MOON AT LOCAL TIME
*SWITCH = DIGITAL OUTPUT FOR MOON IN PRIMARY BEAM
.OADSWTCH = DIGITAL OUTPUT FOR HOT LOAD CALIBRATION
NOSWITCH = DIGITAL OUTPUT FOR ELECTRONIC BASELINE
**SWITCH = DIGITAL OUTPUT FOR SKY-SKY BASELINE
** = TEMPERATURE DIFFERENCE BETWEEN HOT AND AMBIENT LOADS
AGE = AVERAGE DIGITAL OUTPUT
PROBABLE ERROR OF DIGITAL OUTPUT

ACKNOWLEDGEMENT

We wish to acknowledge the assistance of several individuals who assisted us during the period of this contract. Mr. Earl Jackson, Venus Station Manager at the Goldstone Tracking Station, gave much needed support during the lunar eclipse observations and subsequent antenna evaluation tests. Mr. Robert Gardner again assisted us in radiometer development, testing, and maintenance. Mr. Donald Oltmans of USC is responsible for the construction of the radiometer and its associated electronic equipment. He also assisted us during the eclipse observations, radiometer testing, and antenna evaluation. Mr. Bruce Parham of JPL assisted in radiometer development, radiometer noise spectrum studies, and lunar eclipse observations. Dr. Takeshi Sato of JPL gave valuable support and participated in many illuminating discussions regarding the project. Lois Busch of JPL carried out much of the computer analysis of the lunar eclipse results. Mr. Pat Shoals and Mr. Randy Gutentag of USC assisted during radiometer testing and lunar eclipse observations.